Commucation No.
TUSSC--2011/1

MODELING RESERVE SYSTEM PERFORMANCE FOR LOW-DUCTILITY BRACED FRAMES

by

MARYAM ABOOSABER

CAMERON R. BRADLEY

JESSALYN M.R. NELSON

ERIC M. HINES

Final Communication Submitted to:
the American Institute of Steel Construction
under the Contract: "Moderate Ductility Dual Systems and Reserve Capacity"

December 2012

Tufts University Structural Systems Communication (TUSSC)
Department of Civil and Environmental Engineering
200 College Avenue
Medford, Massachusetts 02155

TABLE OF CONTENTS

LIST OF FIGURES

1. Introduction

Designers in the East attempting to develop lateral systems that address moderate seismicity both safely and cost-effectively often find themselves constrained by code requirements that do not provide the flexibility that is available in the West (Hines and Fahnestock 2010). Many concentrically braced frame (CBF) buildings are currently designed using a response modification coefficient, R, equal to 3, which allows seismic detailing to be ignored. This approach has not been proven to guarantee acceptable seismic performance. Using R = 3 can result in design forces in the building and its foundations that are higher than forces resulting from wind loads, thereby increasing cost without clearly achieving elevated performance. Furthermore, it is not uncommon practice in moderate seismic regions to take a conservative approach to CBF design by specifying larger member sizes and larger forces than required for an R = 3 approach. In such cases, where the braces are oversized and the rest of the lateral system has not been explicitly proportioned according to capacity design principles, this type of conservatism can result in systems that are less safe than systems with weaker braces. In view of these limitations, new design approaches and system configurations may provide designers with opportunities both to ensure better seismic performance and to reduce cost. The philosophy behind such systems should enable designers to judge where added cost will most benefit system performance.

Empirical evidence indicates that steel braced frames possess appreciable reserve capacity – in the form of gravity framing and gusset plate connections. These partially-restrained connection elements form a “reserve” moment frame system that can prevent sidesway collapse even when the primary lateral force resisting system (LFRS) is significantly damaged due to brace fracture. When required, reserve capacity can be enhanced without significant expense. As summarized by Hines et al. (2009), collapse performance of CBF systems that possess limited ductility appears to be impacted less by a system’s strength than by its reserve capacity. It is therefore proposed to reconsider the design of braced frames in low and moderate seismic regions as moderate-ductility dual systems. Such dual system behavior can be viewed from two different perspectives:

1. A stiff primary braced frame with a moment frame reserve system to prevent collapse in the event of brace failure.

2. A flexible moment frame stiffened by a sacrificial braced frame designed to withstand wind loads and to provide service-level drift control.

Figure 1.1. Reserve system behavior: (a) Experimental results for the 5th Story of a 0.3 Scale, 6-story CBF tested by Uang and Bertero (1986), as reported by Whittaker et al. (1990); (b) Idealized system force-displacement response of a braced frame with reserve system, showing three key parameters that affect reserve system behavior. illu-

strates the idea behind moderate-ductility dual systems. In contrast to high seismic design, where system ductility is achieved through large component ductility, e.g., plastic hinges, brace buckling or brace yielding, moderate-ductility dual systems achieve system ductility through the coupling of a stiff system with a flexible system. The stiff CBF system is expected to perform in a brittle manner; however, if the flexible system possesses sufficient strength, stiffness and ductility to prevent collapse, then adequate system ductility has been achieved.

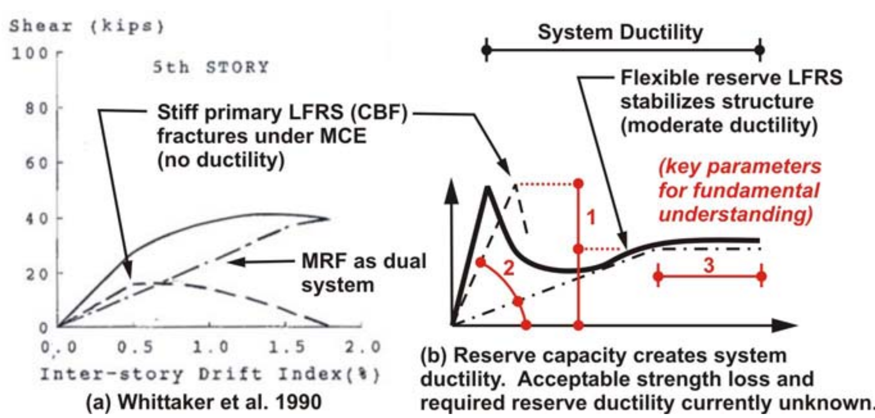

Figure 1.1. Reserve system behavior: (a) Experimental results for the 5th Story of a 0.3 Scale, 6-story CBF tested by Uang and Bertero (1986), as reported by Whittaker et al. (1990); (b) Idealized system force-displacement response of a braced frame with reserve system, showing three key parameters that affect reserve system behavior.

The strength, elastic stiffness and ductility of the reserve system are represented by the numbers 1, 2 and 3 in Figure 1.1(b). It is possible to imagine a successful reserve system that has very little ductility (3) of its own. In this instance, system ductility would be achieved without relying on any component ductility. Figure 1.1(a) shows the performance of the 5th story of a 6-story, 0.3 scale, CBF dual system tested at the University of California, Berkeley in the mid 1980s. To this authors' knowledge, these are the only published test results demonstrating the experimental performance of reserve system capacity based on a large-scale shake table test. Figure 1.1 (a) differs significantly from Figure 1.1 (b) in that the reserve system is nearly as stiff, and significantly stronger than the primary CBF. Since the testing at Berkeley was part of a larger joint research venture between the U.S. and Japan in the 1980s, this design resulted from design criteria assembled to satisfy both U.S. and Japanese building codes that were then current. Considering the strength, stiffness and ductility of reserve systems as shown in Figure 1.1 (b) as fundamental to collapse performance of low-ductility steel CBFs, it becomes clear that the significant stiffness and strength discontinuities in such systems present challenges for the proper analysis of these systems. Furthermore, considering that collapse is the performance level in question for such systems, the ability of such analyses to predict collapse becomes of paramount importance. The interconnected nature of this problem, which includes low-ductility system performance, appropriate ground motion suite selection and careful consideration probabilistic methods for collapse risk assessment has been discussed at length by Hines et al. (2009, 2010, 2011). Ongoing large-scale component testing by Stoakes and Fahnestock (2010, 2011) has demonstrated that reserve capacity may be designed into standard braced frame gusset plate connections for relatively little cost, and work is underway to assemble the resources necessary for shake table testing of low-ductility CBFs with reserve systems at large-scale or full-scale.This report discusses the results of analytical work conducted since the printing of Hines et al's 2009 paper. Recognizing the problematic nature not only of assessing the non-linear dynamic behavior of these systems but also of making these assessments up to the point of system collapse, the authors have attempted to re-frame the question of reserve system behavior on a fundamental level. Models have been simplified in order to isolate the key strength and stiffness discontinuities between the primary CBF and the reserve system. These simple models have been constructed in two different software packages, Ruaumoko (Carr 2004) and OpenSees (2007) in an attempt to distinguish issues related to physical collapse from issues related to numerical convergence.

After discussing the challenges of modeling braced frames with reserve systems, this report introduces a discussion on partially restrained moment connections that could be used with existing gravity framing to create reliable and efficient reserve systems. A preferred connection for “Type II construction” (Disque 1976, Geschwinder and Disque 2005) PR-connections that consist of bolted top and seat angles with bolted double web angles have the ability to provide significant moment-rotation capacity in gravity framing connections for very little added cost. These connections and their use in Type II construction have a long and interesting history that has focused primarily on their use for resisting wind loads in the elastic range. This report and this research approaches these connections with a primary interest in their ultimate moment and rotation capacity and its potential to enhance gravity system lateral reserve capacity economically.

2. SUNY Buffalo Moment Frame Test

In preparation for modeling low-ductility CBFs with reserve systems, models were created to assess the performance of the 4-story small scale moment frame that was recently tested to collapse at the NEES facility at the State University of New York (SUNY) in Buffalo (Lignos 2008). In this research, a 1:8 scale 4-story moment frame was tested up to collapse, and compared to modeling results based on Drain 2D software. A schematic diagram for this test, as reported by Lignos (2008) is shown in Figure 2.1. Figure 2.2 shows the comparison, made by Lignos (2008) of the experimental and analytical incremental dynamic analysis (IDA) results. Based on these results, Lignos et al. concluded that "prediction of collapse is feasible using relatively simple analytical models provided that component deterioration is adequately represented in the analytical model" (Lignos et al. 2010, Summary).

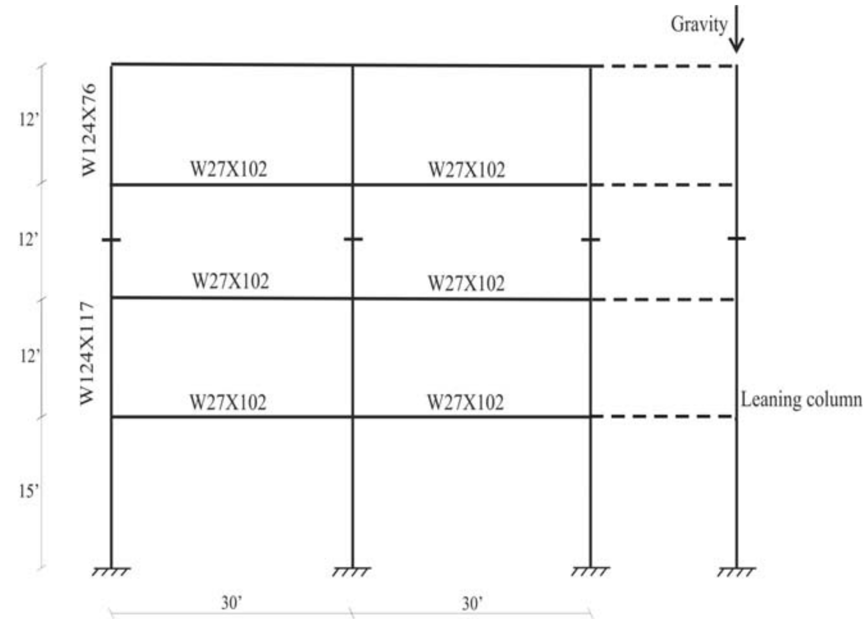

Figure 2.1. Schematic of 4-story moment frame prototype on which 1:8 scale test frame was based.

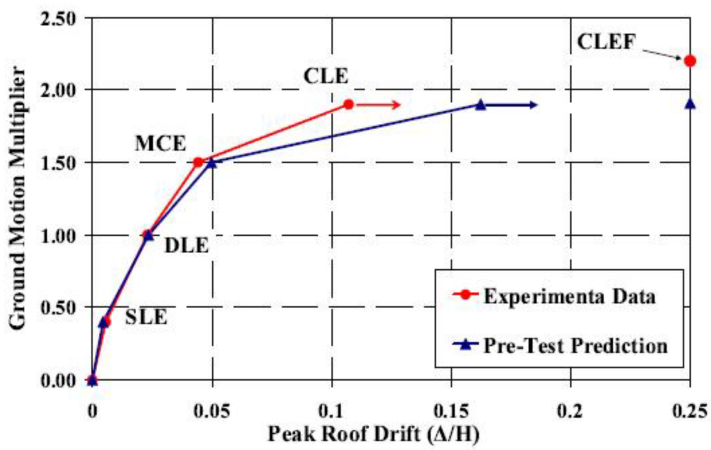

Figure 2.2: Buffalo Frame IDA Comparison (Lignos 2008, Figure 7.26).

Rotational springs were used to model the hinge areas of beams and columns. The P-Delta load was applied to the leaning column which was modeled as an elastic beam column element and connected to the frame using truss elements. The P-Δ geometric transformation was used to include the large displacement in the model. In the Ruaumoko model, a bilinear inelastic hysteresis rule was used to model nonlinear behavior of the beams, assuming ILOS=0 implying no strength degradation. This model also has an elastic beam column element with large area to model the leaning column which is connected to the frame by a rigid link.

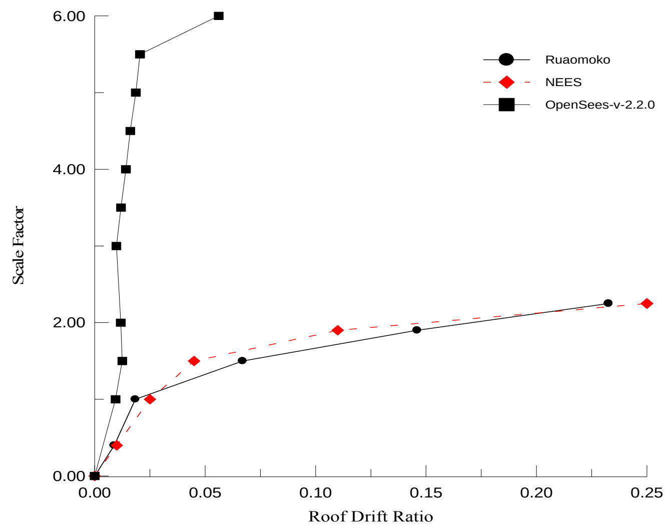

Figure 2.3. Buffalo Frame IDA Comparison (Experiment (NEES), Ruaumoko, OpenSees V.2.2.0). OpenSees analysis time step differs from input time step.

Figure 2.3 shows the IDA comparison between the experimental Buffalo frame, OpenSees and Ruaumoko. In this figure, OpenSees shows significantly larger collapse capacity with respect to two other results. The erroneous OpenSees results could be explained by the fact that the analysis time step (θ_{ta} = 0.005s) differed from the input ground motion time step (θ_{tgm} = 0.01s). Figure 2.4 shows the IDA curve for the OpenSees model with compatible time steps. This model experienced convergence problems at even small scale factors (SF=0.2). After discussion of this issue with Lignos, the same model was run in a different version of OpenSees (Version 2.2.2.e). The IDA comparison between OpenSees V.2.2.2.e, Ruaumoko and experimental data is showed in Figure 2.5. It can be seen that the IDA curves have significantly better correlation.

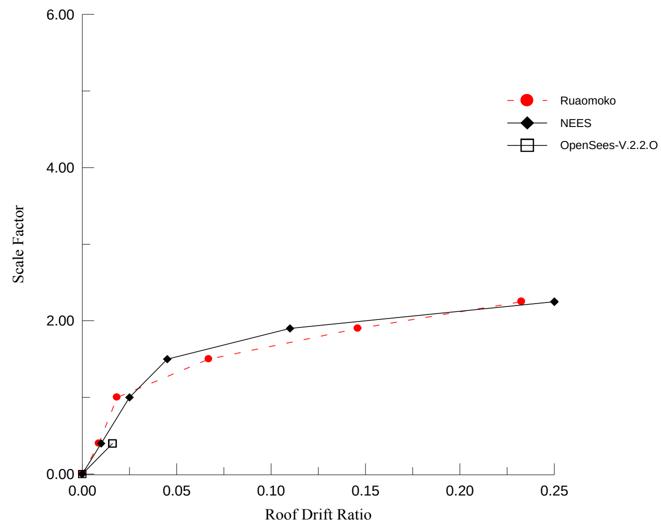

Figure 2.4. Buffalo Frame IDA Comparison (NEES, Ruaumoko, OpenSees V.2.2.0). OpenSees analysis time step is the same as the ground motion input time step.

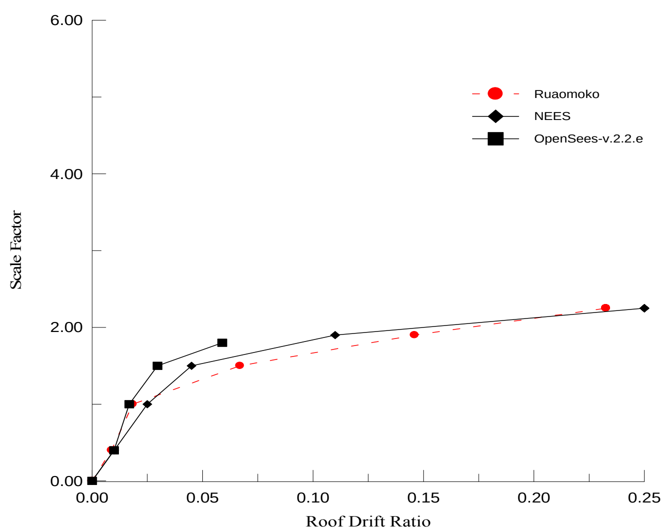

Figure 2.5. Buffalo Frame IDA Comparison (Experiment (NEES), *Ruaumoko*, *OpenSees V.2.2.2.e*). *OpenSees* analysis time step is the same as the ground motion input time step

3. One-Story System Analysis

3.1 Scope

In an effort to establish benchmarks for the comparison of Ruaumoko and OpenSees, a series of 1-story models were created. These models are:

-Single Cantilever

-Moment Resisting Frame (MRF)

-Eccentrically Braced Frame (EBF)

-Low-Ductility Concentrically Braced Frame (CBF)

While this research is concerned primarily with the performance of Low-Ductility CBFs, the difficulties in modeling such frames up to collapse led to the decision to establish baseline models of more ductile systems. Results from these models (presented in Sections 3.3 through 3.5) demonstrate a high degree of consistency between Ruaumoko and OpenSees for dynamic analysis of materially and geometrically non-linear systems. When compared to results for the low-ductility CBF in Section 3.6, the consistency in these more traditional, ductile systems helps to emphasize the uniqueness of low-ductility CBFs with reserve systems in terms of collapse performance and modeling. The large discontinuities in stiffness and strength experienced by these systems pose modeling challenges that simply are not present in more traditional systems.

3.2. Ground Motions

Ground motions for this study are taken from the previous study by Hines et al (2009) and Hines et al (2011). A detailed description of the suite of ground motions referenced in the 2009 paper can be found in Hines et al. (2011). Since the present study is concerned more with comparisons between analytical methods than with probabilistic performance assessment, it features only three of the ground motions from the previous studies: Ground Motions (GM) 4, 8 and 12. The acceleration response spectra (ARS) curves for these three ground motions, amplified according to a typical Boston Site Class D soil profile (Hines et al. 2011, Sorabella 2006) are shown in Figure 3.1.

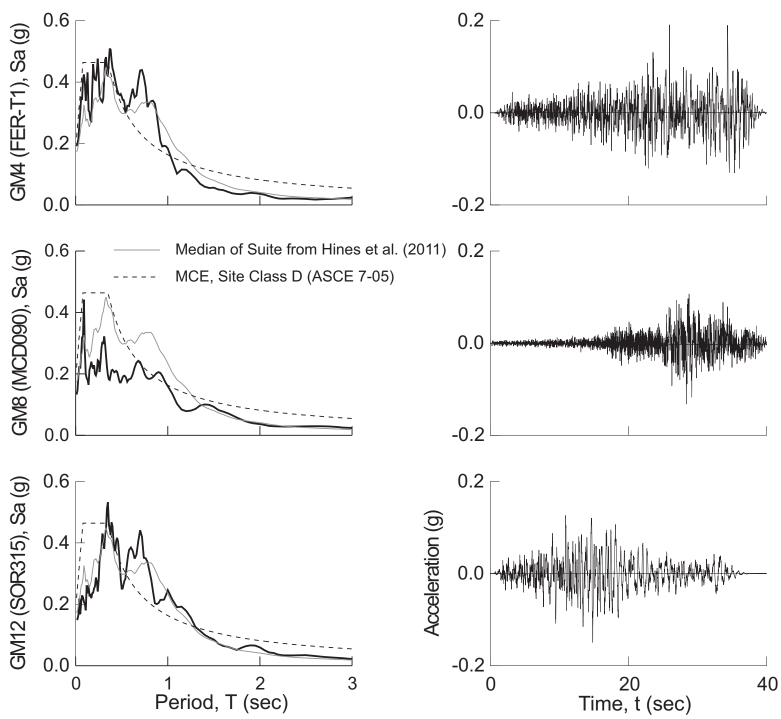

Figure 3.1. Ground motions and acceleration response spectra used for this study.

3.3 Cantilever

3.3.1. Model Setup

The first system is a simple cantilever which forms a plastic hinge at the base, shown in Figure 3.2. This cantilever represents the reserve system of other simple models which is equivalent to the moment frame of the first story of the nine story model (for ¼ of the building, see chapter 4). To find the equivalent section a push over analysis was done on the first story of the nine story model and non-linear force-displacement response of the cantilever including P-Δ effects was calibrated to approximate the pushover curve for the first story of the 9-story building reserve system. Instead of adding a second leaning column to assume the remainder of the building weight, the area of the leaning column was increased to maintain axial stresses similar to the first floor graving framing columns. The resulting section is approximately 10.2 in. deep and 46 in. wide. The column vertical load is approximately equal to ¼ of the nine story building. The column material is steel, with E = 29,000 ksi, Fy = 46 ksi, and a linear strain hardening modulus of Esh = 290 ksi. Note that these numbers were chosen to approximate the force displacement behavior of the first story reserve system, not to model an actual steel column. For this reason, it is not necessary for the cantilevered column in Figure 3.2 to be considered realistic in its own right. Figure 3.3 compares the pushover curves for the reserve system in Figure 3.2 and the first story reserve system for ¼ of the 9-story building. For the assessment of the first story reserve system, the second story was also modeled with braces intact so as to allow the gravity columns to contribute to the reserve capacity in addition to the gravity beams. In Ruaumoko, the plastic hinge length was set at half of the column depth or 5.1 in. In OpenSees, the column has 4 fibers along the depth and 16 fibers along the width.

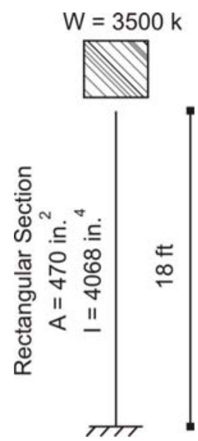

Figure 3.2. Cantilever system

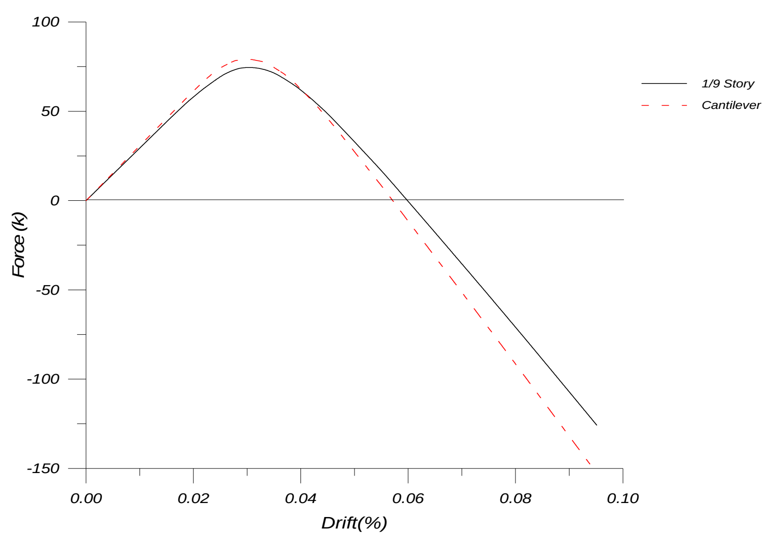

Figure 3.3. Comparison of reserve system pushover curves between SDOF in Figure 4 and the first floor reserve system for ¼ of the 9-story building

3.3.2. Analysis Results

Incremental Dynamic Analyses (IDAs) for this system are shown in Figure 3.4. Performance of this system in Ruaumoko and OpenSees are very similar under GM4, GM8 and GM12, with Ruaumoko predicting slightly higher maximum drifts than OpenSees. Figure 3.5 shows response history analysis (RHA) results in terms of drift as a function of time for both programs under GM8. In this figure, it becomes clear that in addition to predicting slightly higher maximum drifts, Ruaumoko also predicted higher residual drifts. This observation is consistent with observations of other systems.

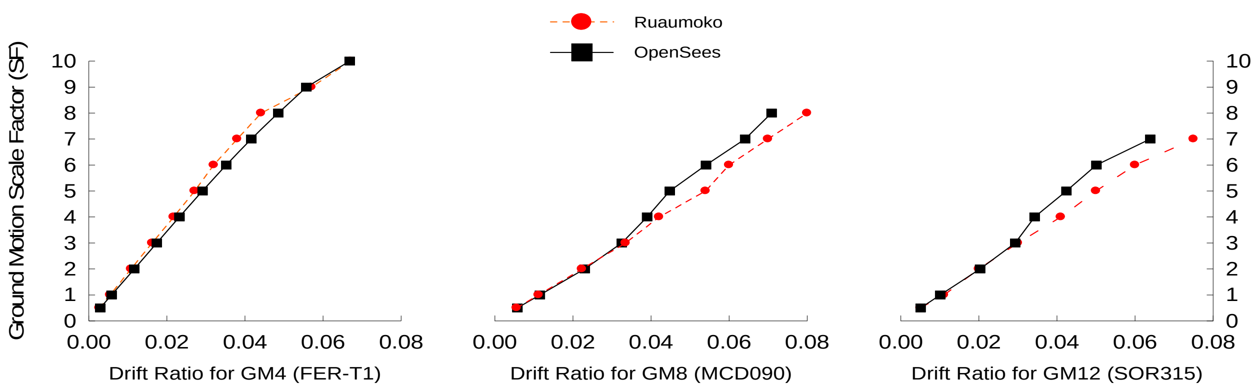

Figure 3.4. Cantilever IDA comparisons for GM4, GM8 and GM12 (*Ruaumoko*, *OpenSees V.2.2.2.e*).

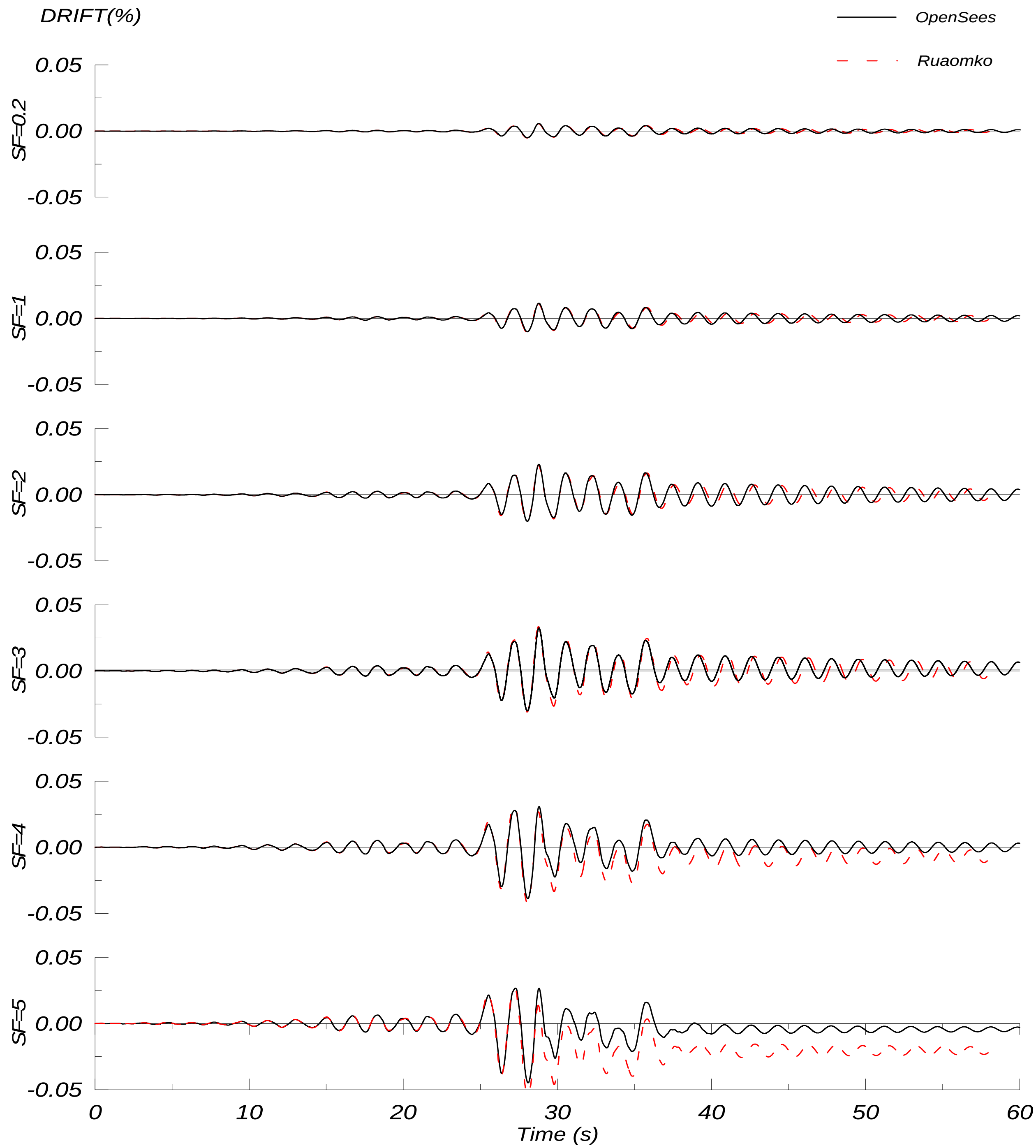

Figure 3.5. Cantilever time history comparison GM8 (*Ruaumoko*, *OpenSees V.2.2.2.e*).

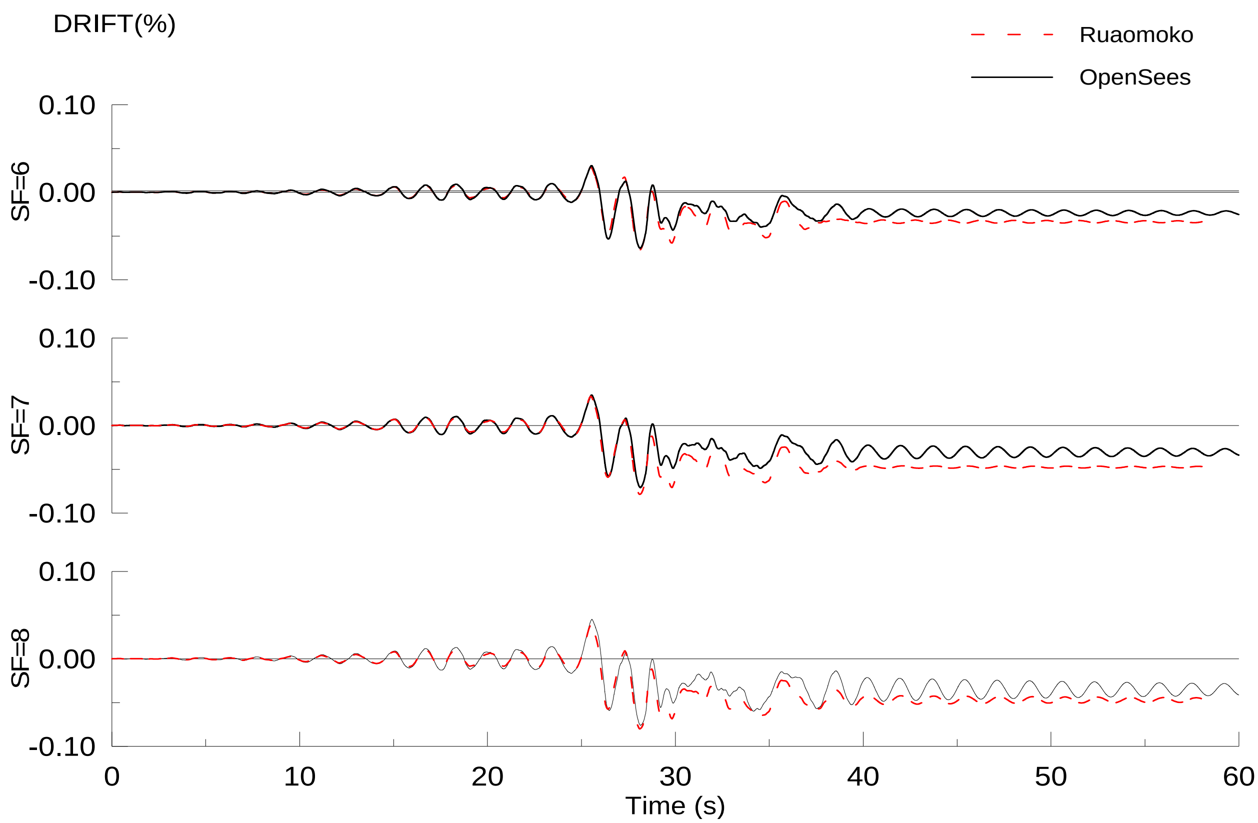

Figure 3.5. (continued) Cantilever time history comparisons for GM8 (*Ruaumoko*, *OpenSees V.2.2.2.e*).

3.4 Moment Resisting Frame

3.4.1. Model Setup

The next simple model which is shown in Figure 3.6 is considered to be a moment frame connected to a cantilever as a reserve system. The reserve system is the same as the cantilever column of Section 3.3. As it will be discussed more in the section 3.6 the braces in the 9-story model are assumed to fracture at a force of 297 kips at their connections prior to buckling. The moment frame is designed to resistant a lateral load equivalent to this fracture force. The material and hinge properties in OpenSees and Ruaumoko are the same as the cantilever model. The P-Δ geometric transformation was used to include the large displacement in the model.

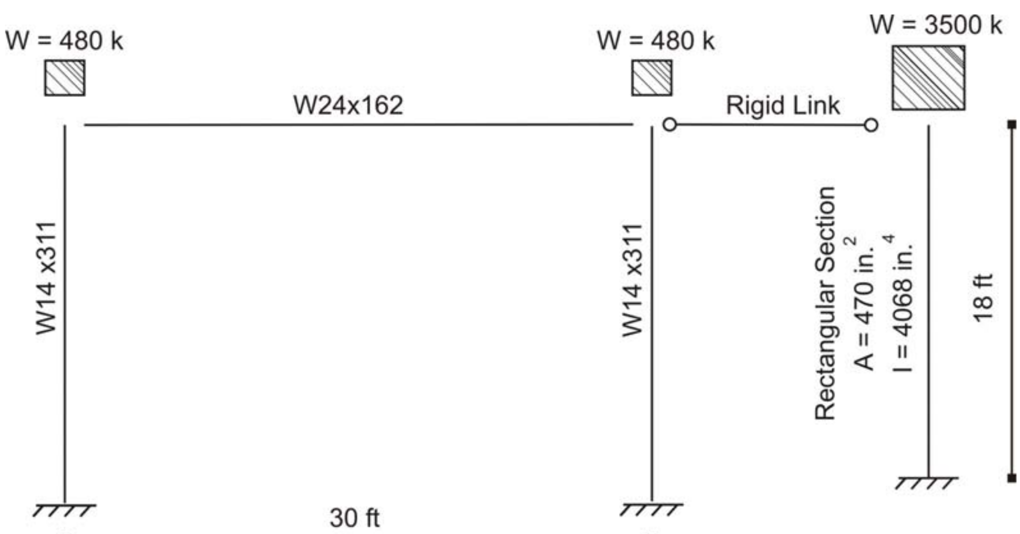

Figure 3.6. Moment Resisting Frame system.

3.4.2. MRF Prototype Design

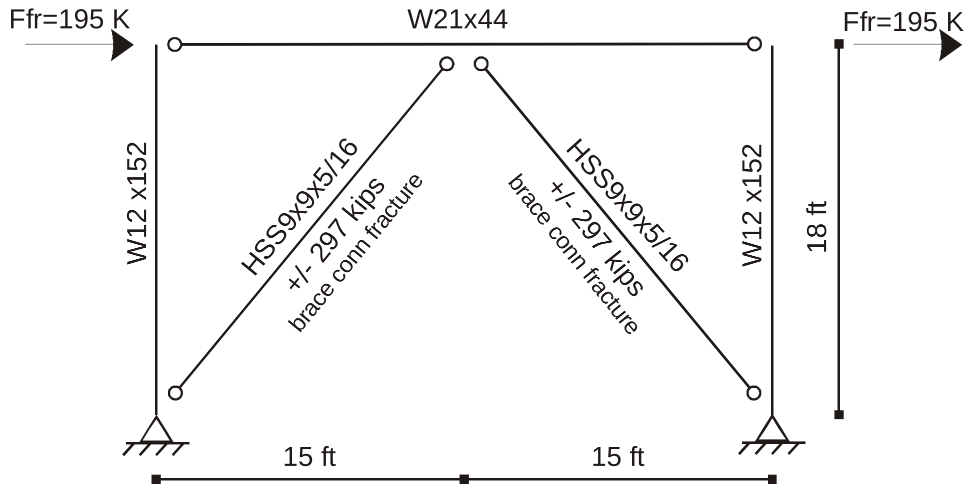

Figure 3.7. CBF fracture force

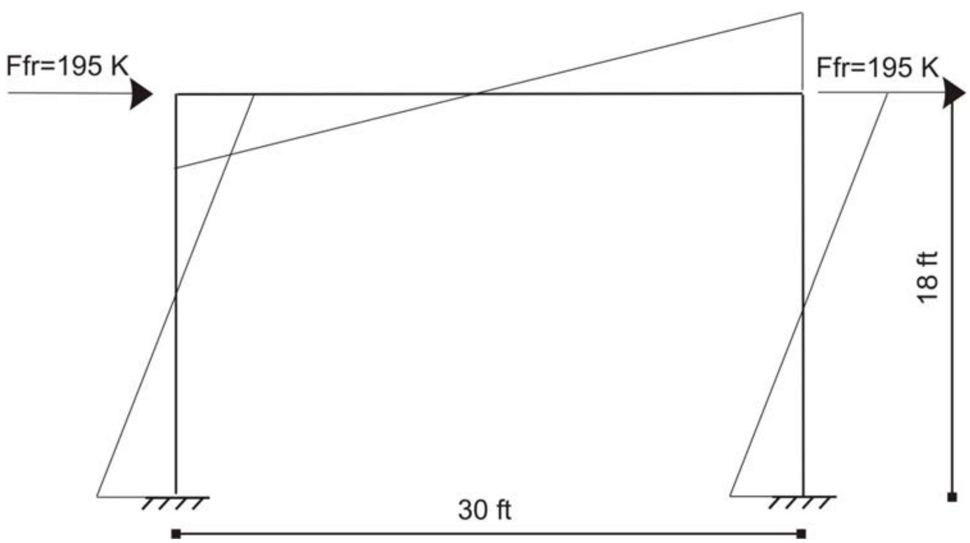

Figure 3.8. MRF moment diagram

$Beam\ Design$:

$$M = 21060\ k - in \quad z_b = \frac{M}{F_y} = 458\ in^3 \quad \Rightarrow \quad W24\ X\ 162$$

$Column\ Design$:

$$Z_c = 1.1\ \times 1.1\ \times 468 = 566\ in^3 \qquad \Rightarrow \qquad W\ 14\ X\ \ 311\ \ (\ Column)$$

$$M = 21060\ k - in$$

$$P = 450\ kips$$

$For\ W14\ X\ 311$:

$$A = 91.4\ in^2 \qquad I = 4330\ in^4 \qquad r = 4.2\ in$$

$$\frac{kl}{r} = \frac{18\ \times 12}{4.2} = 51.4 \qquad F_e = \frac{\pi^2 E}{\left(\frac{kl}{r}\right)^2} = \ 107\ ksi$$

$$F_{cr} = \left(0.658^{\frac{f_y}{f_e}}\right) f_y = 38.58\ ksi$$

$$P_n = 38.58 \times 91.4 = 3526\ kips$$

$$\frac{1.2 \times 450}{0.9 \times 3526} + \frac{8}{9} \times \frac{21060}{0.9 \times 603 \times 46(1 - \frac{1.2 \times 450}{107 \times 91.4})} = 0.963$$

3.4.3. MRF Analysis Results

The IDA comparison for GM4, GM 8 and GM12 can be seen in Figure 3.9. The figure shows a very good match between OpenSees and Ruaumoko results for all three ground motions. The results are shown up to collapse. As it can be seen in the figure, for the GM 4 and GM 8 the instability happen suddenly after the scale factor of 10 and 8 respectively. It’s not clear whether this instability is the result of numerical instability (which can suffer from the quality of code, time step, etc) or if it shows physical collapse. For GM 12, the model is stable up to 8 percent drift ratios in both programs which seems is correspondence to physical collapse. Figure 3.10 shows the drift time history comparison between OpenSees and Ruaumoko for GM 8. As it can be seen in the figure, the results shows very good match, However, for a scale factor 6 and larger, OpenSees shows residual drift after 40th second of ground motion while Ruaumoko doesn’t.

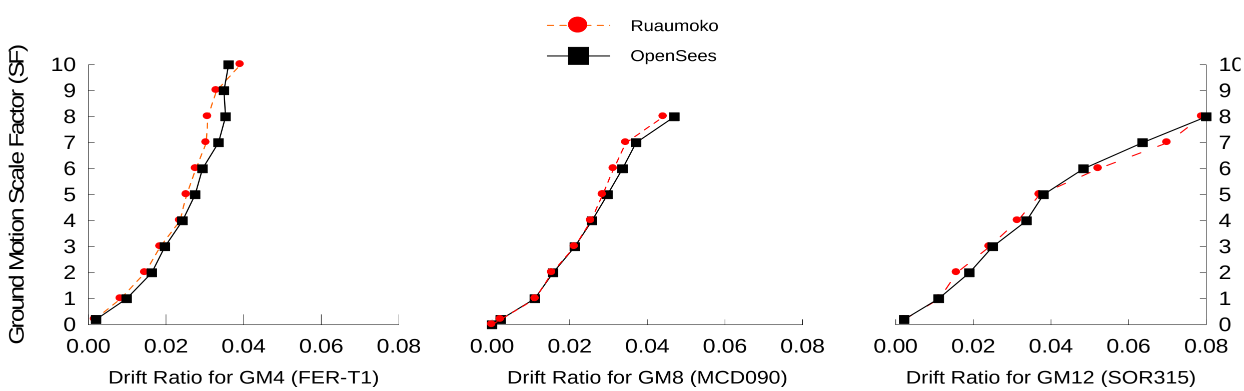

Figure 3.9. MRF IDA comparisons for GM4, GM8 and GM12 (*Ruaumoko*, *OpenSees V.2.2.2.e*).

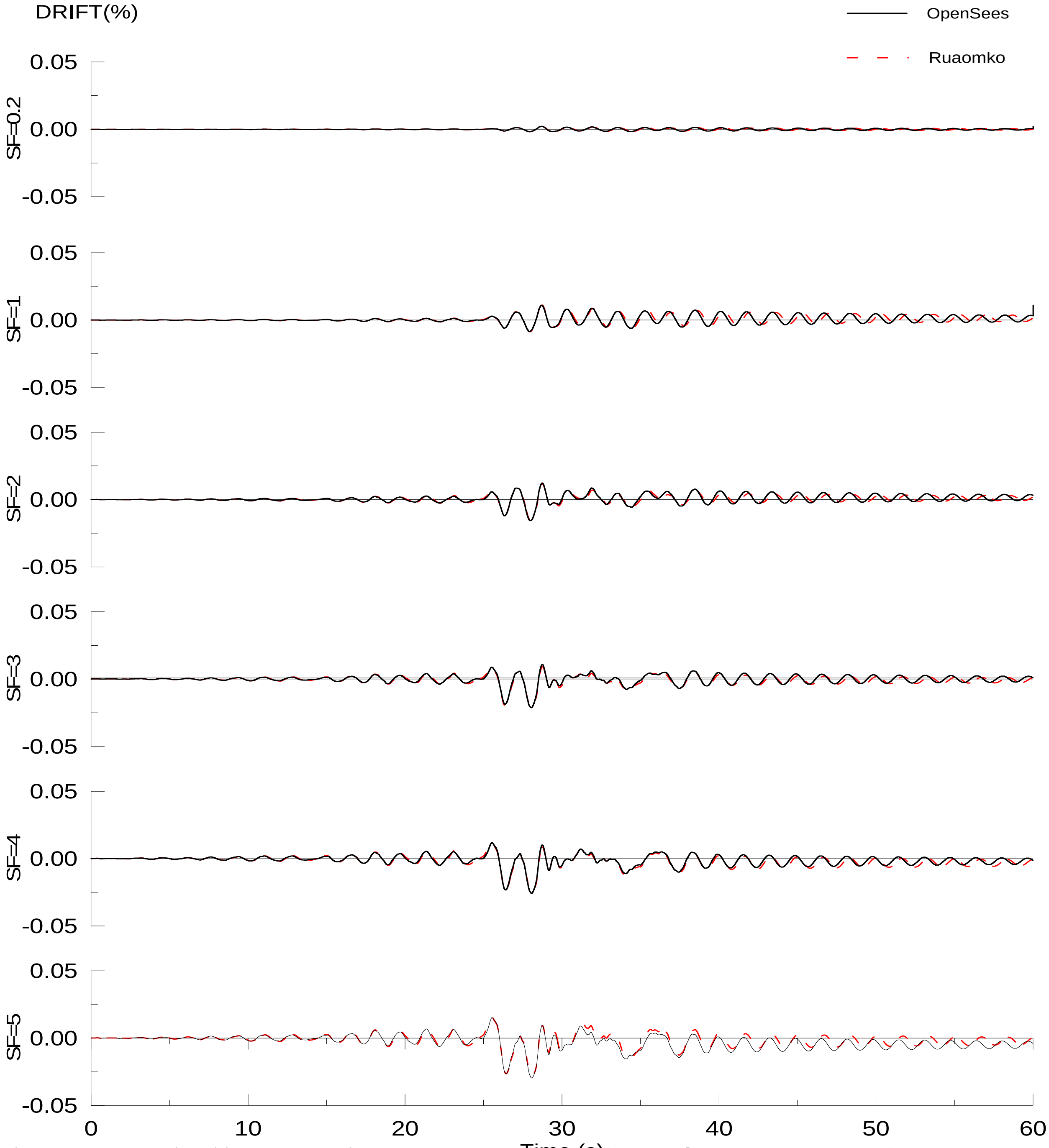

Figure 3.10. MRF time history comparison GM4, GM8 and GM12 (*Ruaumoko*, *OpenSees V.2.2.2.e*).

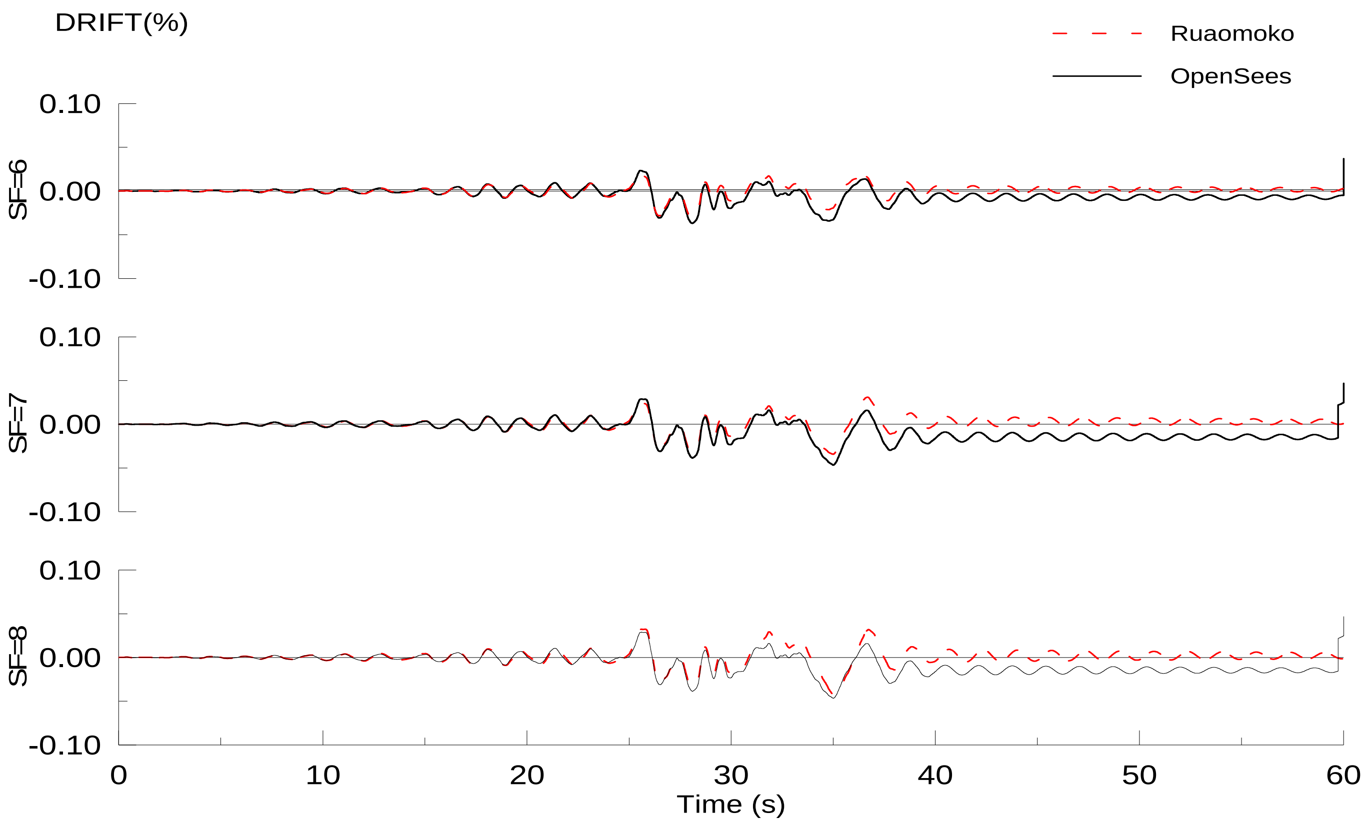

Figure 3.10(Continue). MRF time history comparison GM4, GM8 and GM12 (*Ruaumoko*, *OpenSees V.2.2.2.e*).

3.5 Eccentric Brace Frame

3.5.1. Model Setup

The eccentric braced frame which is shown in the figure 3.11 was designed for the fracture force of braces in the 9 story model (the same design force as moment frame discussed in the section 3.4.1). This model is also has the cantilever of Section 3.3 as the reserve system. In OpenSees all the members are modeled using fiber elements. In Ruaumoko, beam, column and braces are modeled as nonlinear members which forms hinge with the length of half of member size. The shear link in the Ruaumoko consists of six-bilinear rotational spring on each end of the element. More detail about the spring properties can be found in the thesis of Carlo C. Jacob (2010).

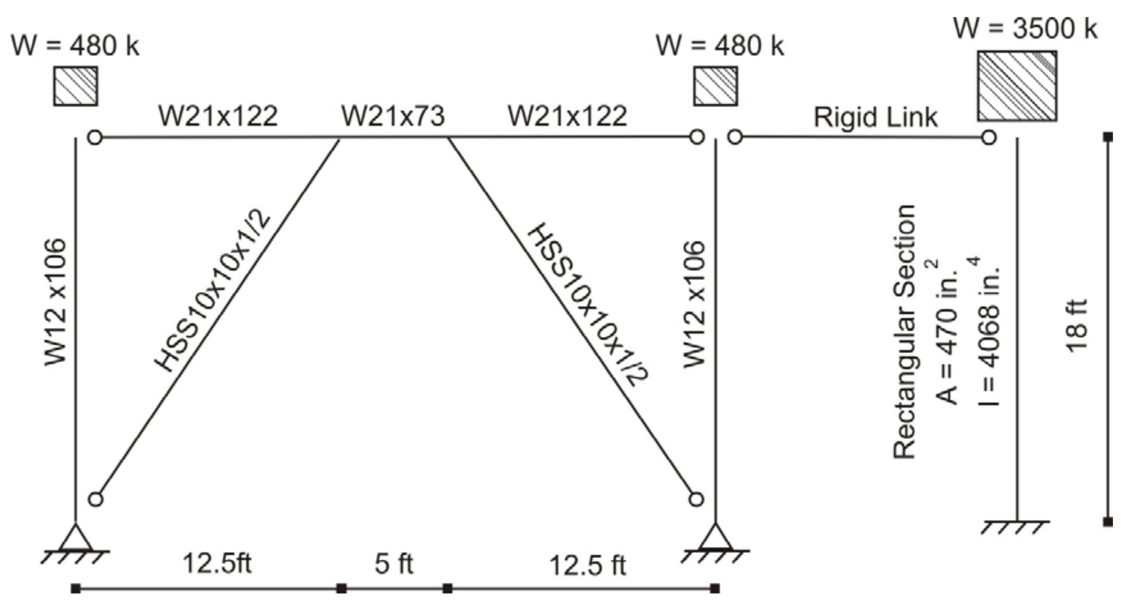

Figure 3.11. Eccentrically Braced Frame system.

3.5.2. Prototype Design

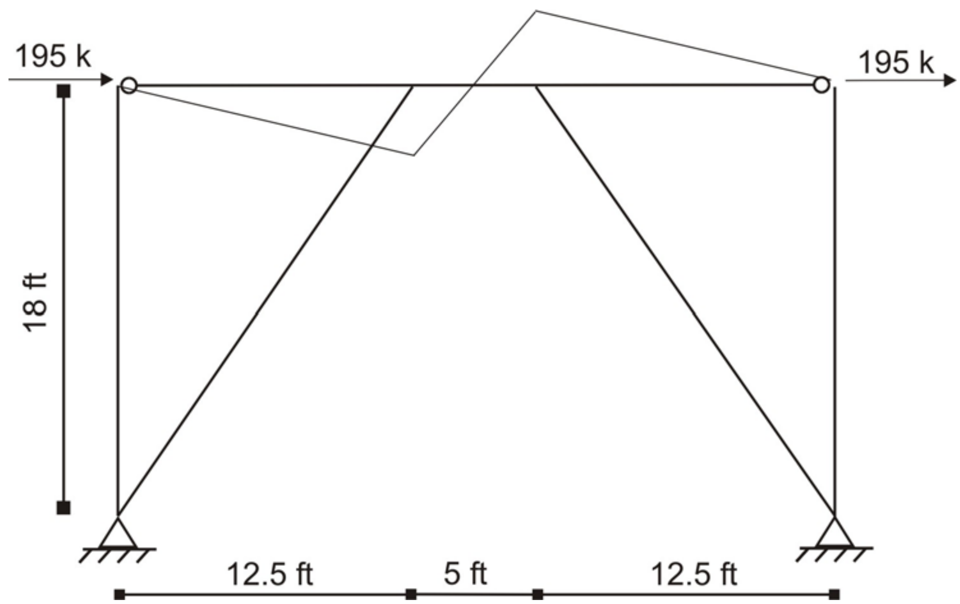

Figure 3.12. EBF moment diagram

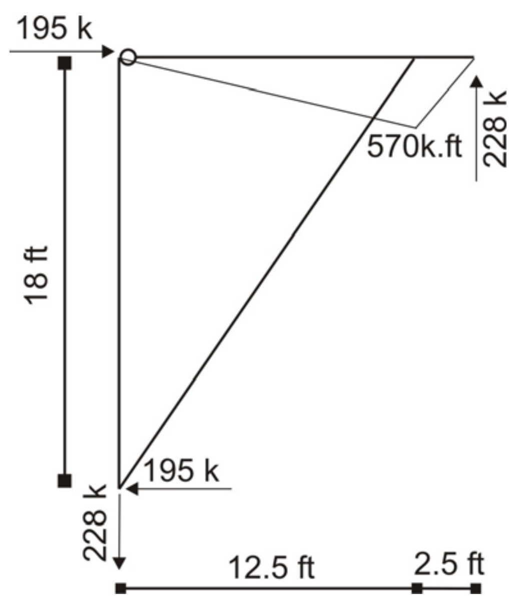

Brace Design:

$$\lambda M_p = 1.1 \times 1.25 \times 172 \times 46 = 11132\ k - in$$

$$\lambda V_l = \frac{11132 \times 2}{60} = 371\ k$$

$$\lambda V_{back} = 371 \times \frac{3}{12} = 92.7\ k$$

$$P_{brace} = (371 + 92.7) \times \frac{21.6}{18} = 556\ k \qquad use\ HSS\ 10\ \times 10 \times 1/2$$

Column Design:

$$\lambda V_l = 371\ k$$

$$P_D = 470\ \ k$$

$$P = 1.2 \times 470 + 371 = 935\ k \qquad use\ W12 \times 106$$

Beam Design:

$$z = \frac{\lambda M_p}{0.9 F_y} = \frac{11132}{0.9\ \times 46} = 269\ in^3 \qquad use\ W21\ \times 122$$

3.5.3. EBF Analysis Results

Figure 3.13 shows the IDA comparison between OpenSees and Ruaumoko for the mentioned EBF model for GM4, GM8 and GM12 . As it can be seen in the figure there is a very good match between these two software results. The results for each ground motions are shown up to the scale factor which is associated with collapse. In this model, the shear link rotation of about 8 percent is considered as the collapse level. The drift time history comparison between OpenSees and Ruaumoko can be seen in the Figure 3.14. This figure indicates that the drift time history response of two models match well together. The only considerable difference between results is the residual displacements. As it can be seen in the figure after 40^{th} second OpenSees shows some residual displacement while Ruaumoko doesn't. A it discussed before, this difference in free vibration zone exists in all other models. It's interesting to note that sometimes OpenSees shows this residual displacement and sometimes Ruaumoko does. Currently the reason of this difference is not obvious for the authors. In EBF this difference also can be seen in the vertical displacement of shear link end nodes which cause some differences in the shear – rotation hysteresis loop of the shear link.

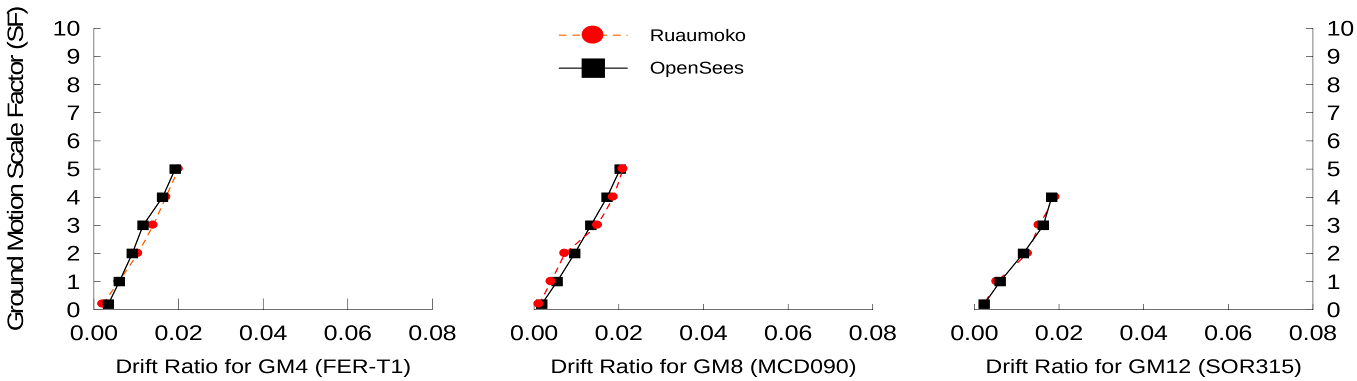

Figure 3.13. EBF IDA comparisons for GM4, GM8 and GM12 (*Ruaumoko*, *OpenSees V.2.2.2.e*).

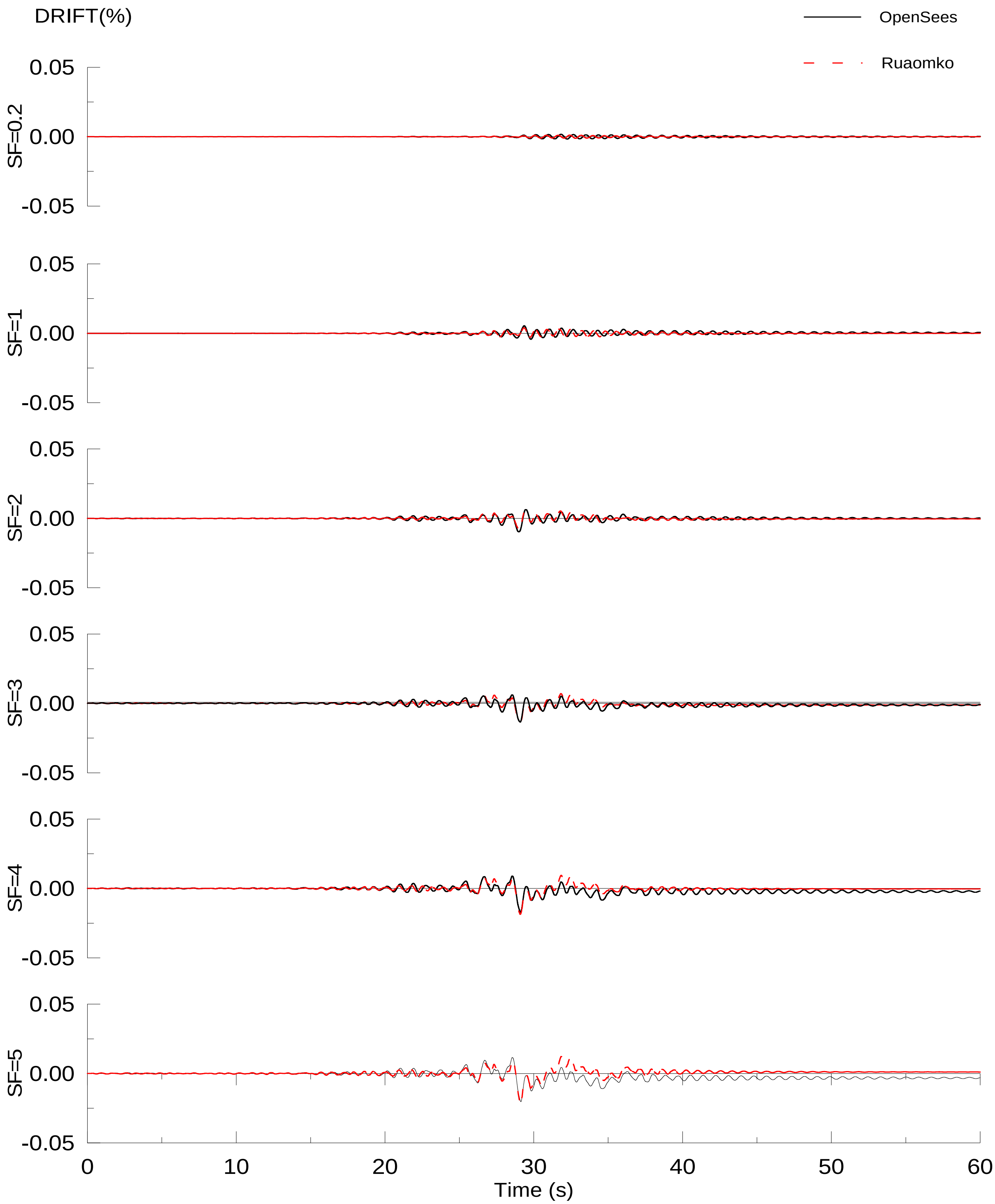

Figure 3.14. EBF time history comparison GM8 (Ruaumoko, OpenSees V.2.2.2.e).

3.6 Low-Ductility CBF

3.6.1. Model Setup

Based on the IDA and displacement time history comparison between OpenSees and Ruaumoko for ductile systems (section 3.3 through 3.5), the nonlinear behavior of these systems can be modeled with high confidence. Figure 3.15 shows the simplified model of the concentrically braced frame created to facilitate comparisons of non-ductile systems between OpenSees and Ruaumoko. The braced frame is similar to the braced frame on the first story of the 9-story building shown in Figure 4.1. Braces are assumed to fracture at a force of 297 kips at their connections prior to buckling. Both braces are modeled to fracture at the same time. This violates the idea that if the braces assume load from the floor above, the compression brace will fracture first, however it simplifies the behavior of the model and allows for more direct study of reserve capacity at a conceptual level. Brace fracture is modeled in Ruaumoko as described in Hines et al. (2009). Brace fracture is modeled in OpenSees by removing the brace from the model (death of the element) after it is subjected to the fracture force.

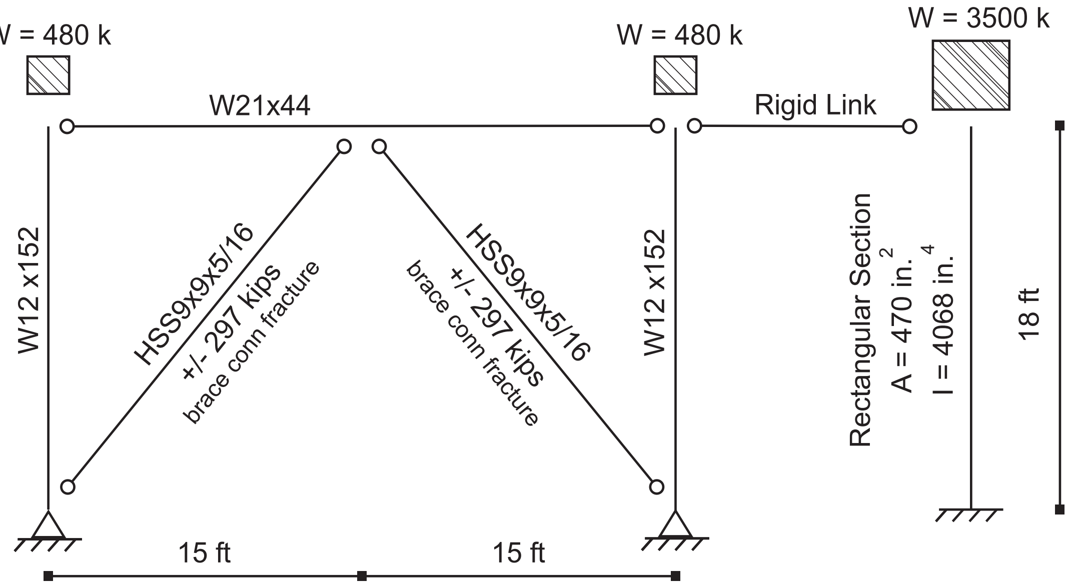

Figure 3.15. Concentrically braced frame system.

Tributary loads for the 9-story building are carried on the braced frame columns as masses, and the remainder of the building mass (for the ¼ building approximated here) is carried on a leaning column, whose non-linear force-displacement response including P-Δ effects was calibrated to approximate the pushover curve for the first story of the 9-story building reserve system.

3.6.2. Analysis Results

Figure 3.16 compares the IDA results using both programs. In general, the IDAs appeared to exhibit similar behavior, however, in many cases the Ruaumoko models would not converge at certain time steps. For this reason, the plots in Figure 3.16 show points only where convergence was achieved. This brought up two interesting considerations: (1) Ruaumoko had appeared to perform more accurately than OpenSees during the calibration study, whereas now OpenSees appeared to be converging more reliably; and (2) these IDAs raised the question as to whether it is possible to see collapse at a lower scale factor and then see resistance to collapse at a higher scale factor.

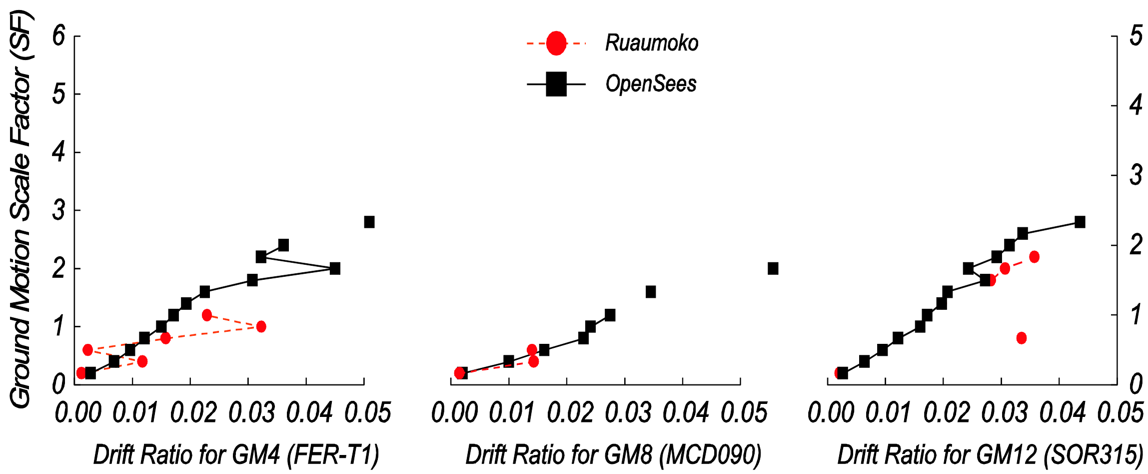

Figure 3.16. SDOF IDA comparisons for GM4, GM8 and GM12 (*Ruaumoko*, *OpenSees V.2.2.2.e*).

Figure 3.16, shows the IDA comparison for the time step of 0.001s. As it can be seen in the figure, Ruaumoko had convergence problem in some of scale factors. In an effort to try to improve convergence of the *Ruaumoko* models, time steps were varied across a spectrum: 0.001, 0.002, 0.003, 0.004, and 0.005. The result of this study was the observation that under different ground motions, the *Ruaumoko* models converged better or worse under different time steps. Smaller time steps did not always yield more consistent results. This led to the intensive calculation of IDA curves assuming every one of the five time steps listed above. The IDAs plotted in Figures 3.18 through 3.20 reflect the selection of the most consistent IDA from the different time step runs.

Figure 3.17 shows the selected time steps for the GM12. To choose the appropriate time step, maximum displacements were compared for different time steps in each scale factor. For small scale factors (elastic range) the analysis was not sensitive to the time step variation. For example for the scale factor of 0.2 the maximum displacement was 0.002 for all time steps. In some of larger scale factors maximum displacements were identical or very close for different time steps. For example for the scale factor of 2 the maximum displacements were changed between 0.030 and 0.032. In this case the difference between maximum displacements is less than 7 percent which doesn't have a significant effect on the IDA curve. In some other cases the results for one or two scale factors were very different with others. For example for the scale factor of 1, the model is unstable for the time steps 0.001, 0.002 and 0.004 and it is 0.0193 for time steps 0f 0.003 and 0.005. In these cases, the maximum displacement of the model in the working time step was used in the IDA curve. As it can be seen in figure 3.17 in some scale factors, the model was unstable for all the selected time steps.

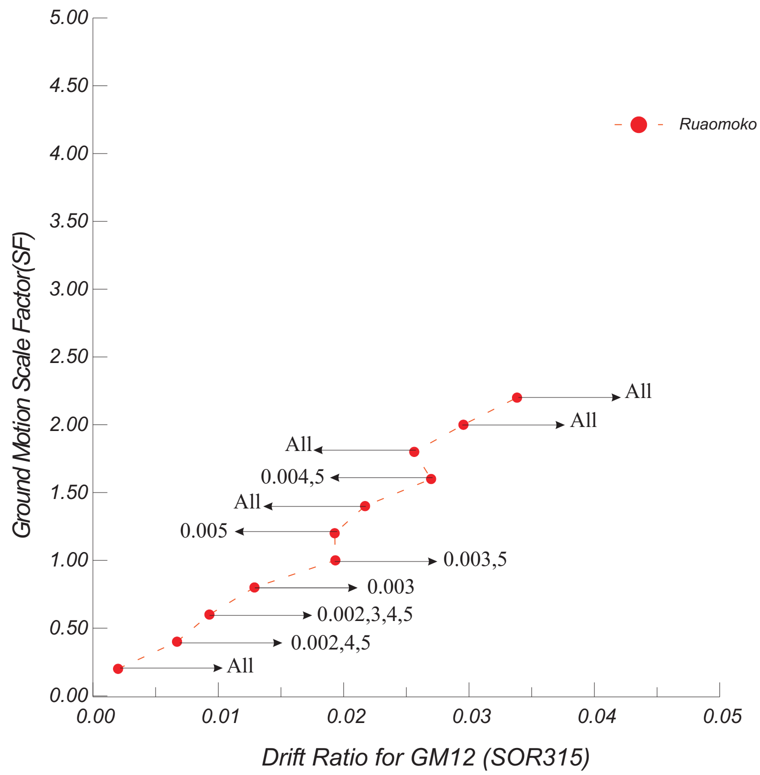

Figure 3.17. Selected analysis time step for Ruaumoko model for GM12.

Figure 3.18 shows dramatic improvement in the convergence of the Ruaumoko models based on the selection of appropriate time steps Currently, it is not clear why variation of the time step—sometimes as an increase, sometimes as a decrease, ensures better convergence of the Ruaumoko models. It is also not clear why the OpenSees models appear to be more stable in the context of this SDOF reserve system when they appeared to perform worse than the Ruaumoko models during the calibration study with the Buffalo frame. Figure 3.18 still shows some non-convergence at lower scale factors and then resumed convergence at higher scale factors. Currently, it also remains unknown whether this non-convergence is numerical or whether it represents physical collapse.

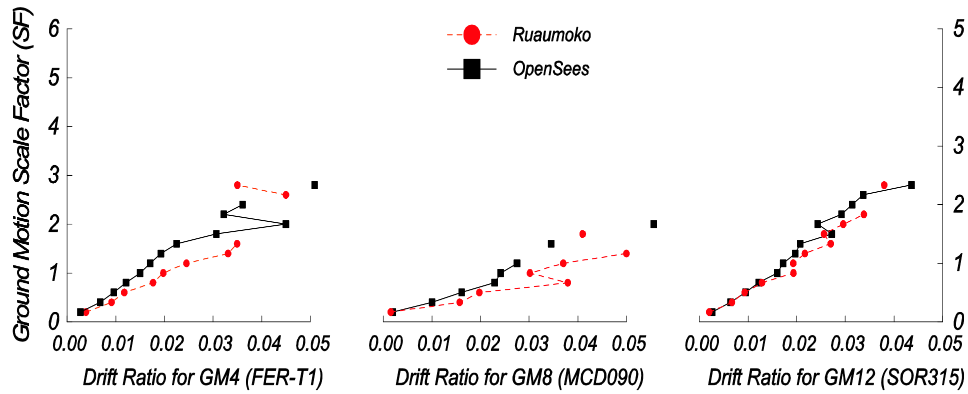

Figure 3.18. SDOF IDA Comparisons for GM4, GM8 and GM12 with refined use of time steps for Ruaumoko.

Figure 3.19 shows results very similar to those reported by Hines et al. (2009) when the reserve system strength and stiffness are doubled. Increasing the reserve system capacity yields dramatic improvement in collapse capacity assessed according to the method of incremental dynamic analysis. For each of the ground motions shown, doubling the reserve capacity yielded increases in collapse capacity of 50% to 100%. On the same note, cutting the reserve system strength and stiffness in half reduced collapse capacity uniformly by more than a factor of 2. Hence, while some mysteries regarding numerical convergence of these models with large stiffness and strength discontinuities remain unsolved, the relationship between reserve capacity and collapse resistance appears to be very clear, with consistent results based on independent models in different software packages.

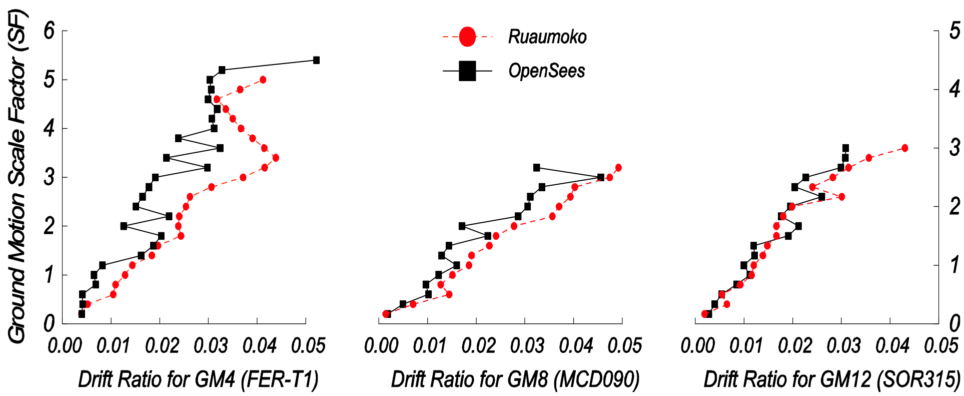

Figure 3.19. CBF IDA Comparisons for GM4, GM8 and GM12 with refined use of time steps for Ruaumoko. Reserve system strengths and stiffnesses are doubled in comparison with the IDAs shown in Figure 3.18.

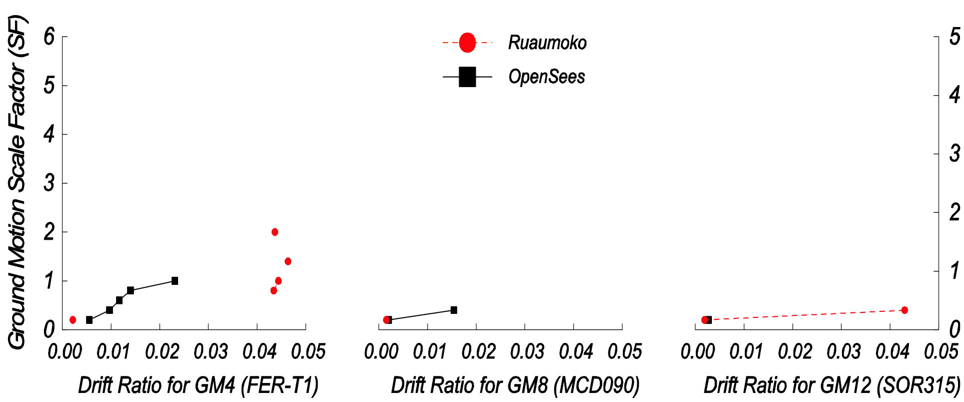

Figure 3.20. CBF IDA Comparisons for GM4, GM8 and GM12 with refined use of time steps for Ruaumoko. Reserve system strengths and stiffnesses are halved in comparison with the IDAs shown in Figure 3.18.

Figure 3.21 and Figure 3.22 shows the displacement time history comparison between OpenSees and Ruaumoko for the one story braced frame. As it can be seen in the figure, the results don't match as well as ductile systems though the maximum displacements are close. It's interesting to note that in this model Ruaumoko shows residual displacement but OpenSees does not.

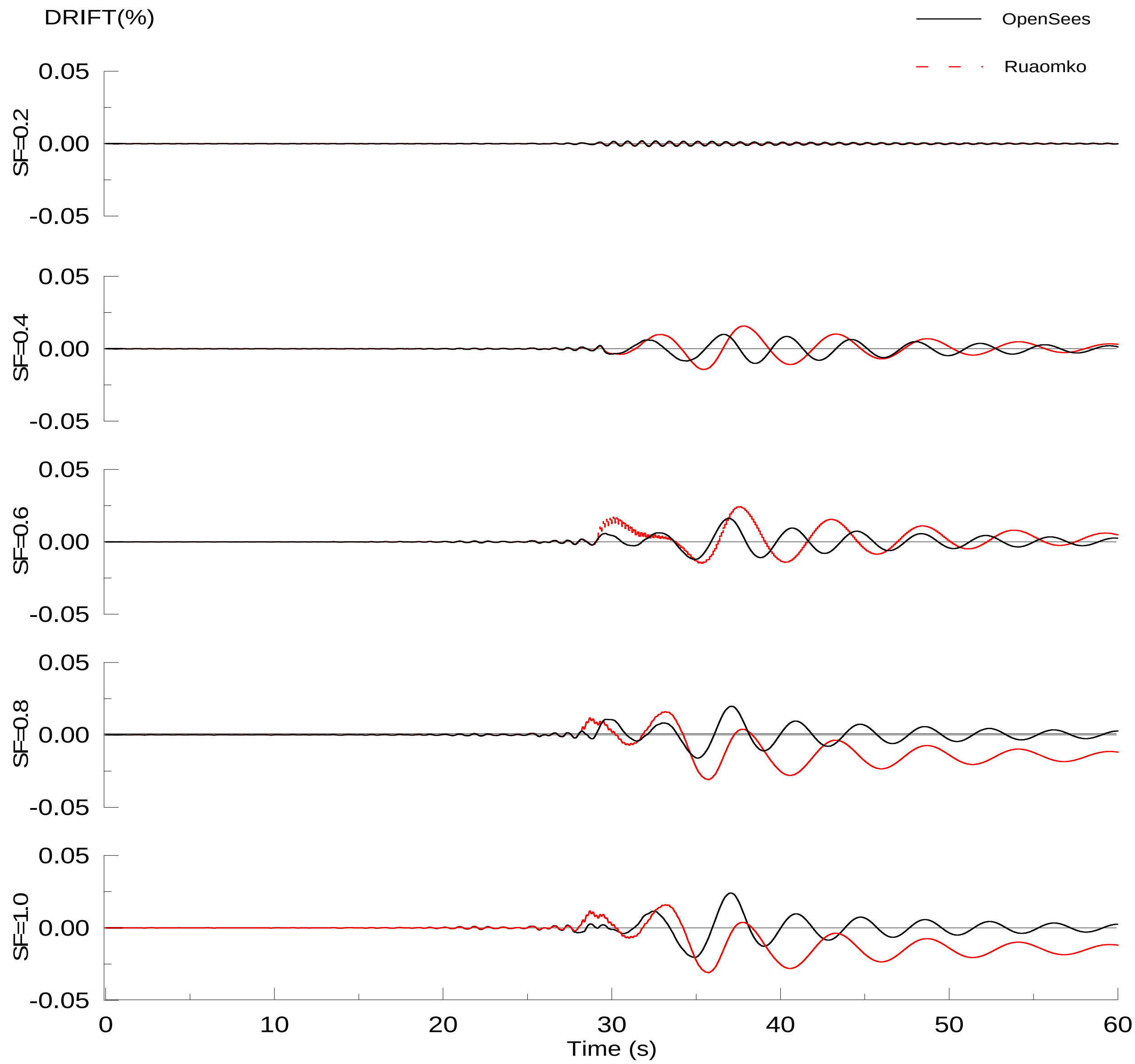

.Figure 3.21. CBF time history comparison GM8 (*Ruaumoko*, *OpenSees V.2.2.2.e*).

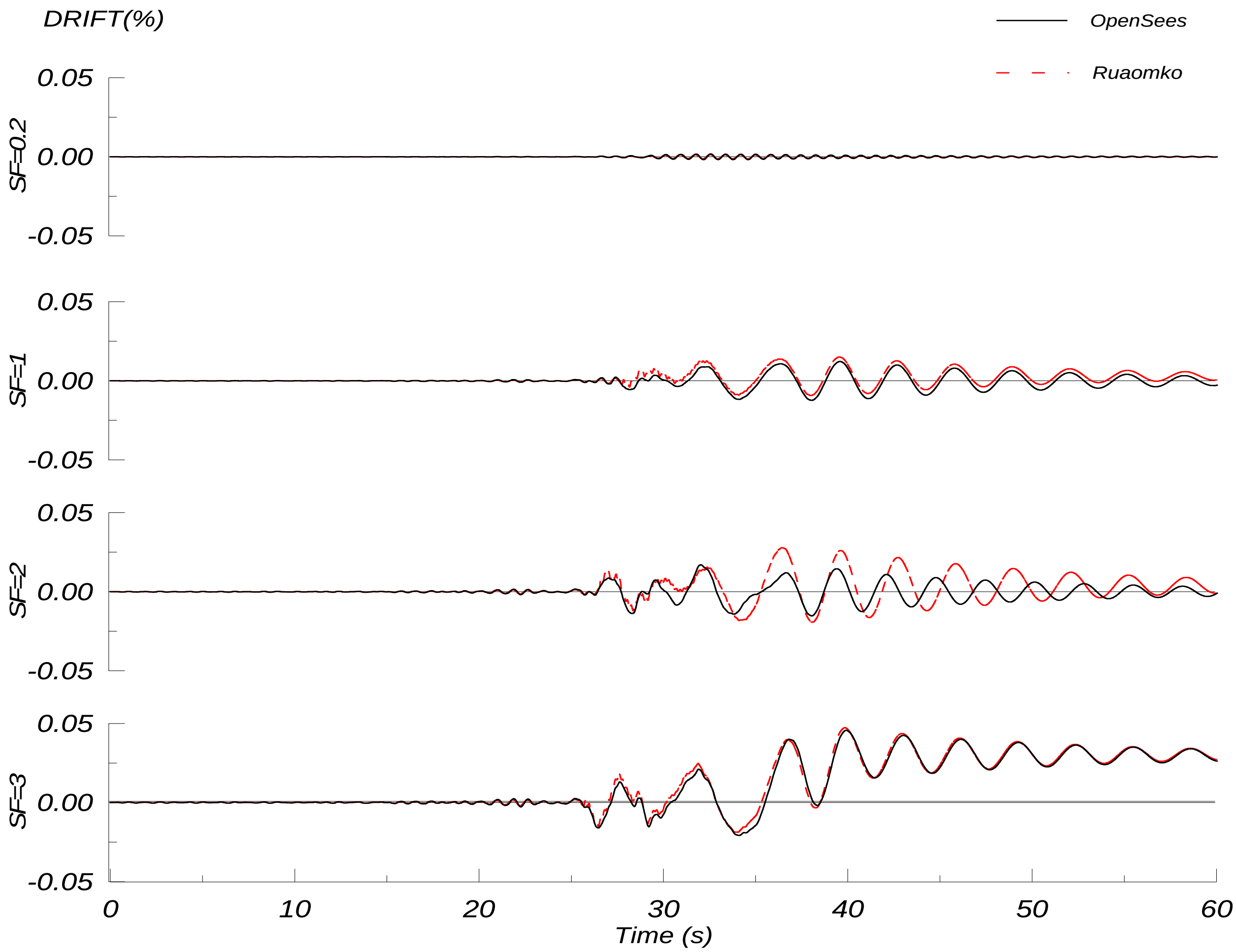

Figure 3.22.Time history comparison for CBF with double strength and stiffness,GM8 (*Ruaumoko*, *OpenSees V.2.2.2.e*).

Though the correlation shown in Figure 3.21 between two software packages is not as close as it was for the ductile systems, it may be possible to achieve better correlations with further refinements to the models, such as higher fidelity material modeling and updates to system stiffness at each time step. An integrated experimental and analytical work was done by Rodgers and Mahin (2004) to investigate the effects of various forms of degradation on the system behavior of moment frames and results indicated that the details of response time history and residual displacements were very sensitive to the connection deterioration assumptions. Therefore, while the effects of sudden changes in the strength and stiffness of the system still remain for low ductility braced frames, better correlation may be achieved by using more similar material property in two software packages. Yazgan and Dazio (2006) showed that residual displacement also can significantly be influenced by element modeling approach. They modeled a reinforced concrete cantilever in OpenSees and Ruaomoko software packages using distributed and lumped plasticity elements and they concluded that residual displacement is sensitive to element properties. Also they showed that properly updating stiffness is crucial for estimating the residual displacement. Improvements to the low-ductility braced frame models based on these and other studies are part of ongoing work to establish appropriate modeling protocols for these systems.

4. Nine-Story System Analysis

4.1. Model Setup

The 9 story model is based on the SAC nine story building (SAC, 2000b), with two braced frame in each side (figure 4.1). The story height is18 ft for the first story and 13 ft for other stories and the span lengths are 30 ft. The building is designed assuming R=3 for Boston, Massachusetts in accordance with IBC 2006 and ASCE 7-05 using Load Resistant Factor Design. The wind loads were determined using exposure B and the seismic load were determined using site class D and seismic design category B. More detail can be found Hines et all (2009).

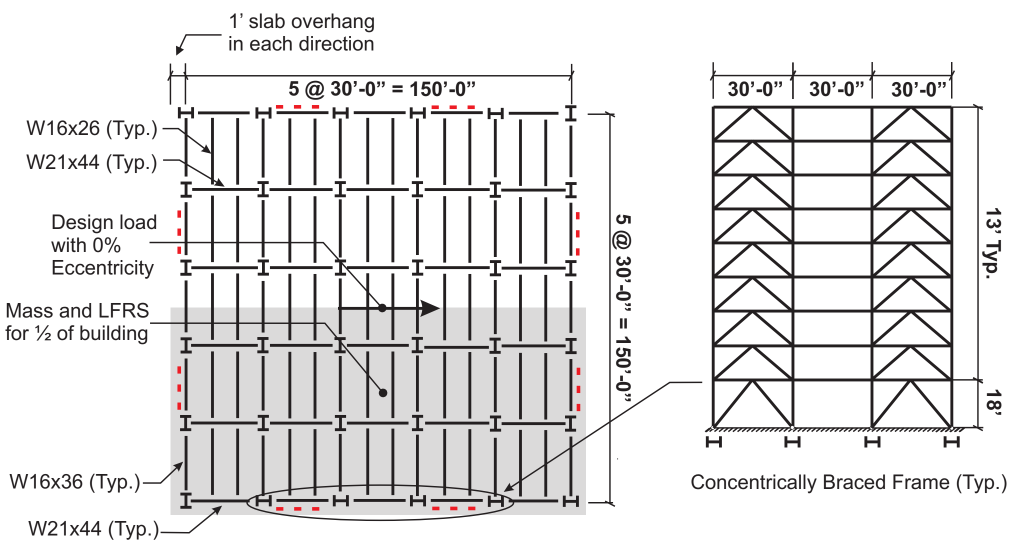

Figure 4.1. 9-story building designed assuming R = 3 as reported in Hines et al. (2009).

Like the simple models, braces are assumed to fracture at the 297 kips force level. In Ruaumoko, beam and column are modeled using hinge element with the length of half of the member sections and in OpenSees fiber elements are used to model nonlinear elements.

4.2. Analysis Results

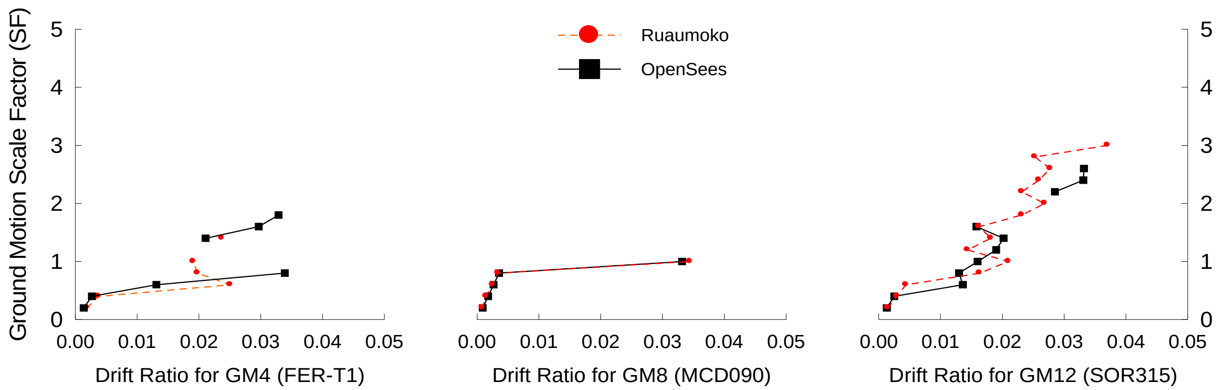

Figure 4.2. 9-story IDA Comparisons for GM4, GM8 and GM12.

It is interesting to note, however, that in the case of the 9-story model, *OpenSees* appears to have had more trouble converging than *Ruaumoko*. This is similar to the observations made during the calibration study on the 4-story Buffalo frame, however it differs from the observations made on the SDOF studies, where *OpenSees* showed more consistent convergence. For this reason, it is difficult to conclude that one program should be preferred to another for this type of analysis, and it seems reasonable to insist that both programs continue to be used in future studies until a clear explanation can be offered regarding the reliable convergence of such models up to the point of collapse.

In general, the 9-story model exhibited lower collapse resistance than the SDOF model featured in Figure 3.15. There is, however, significant variation in collapse resistance between ground motions. The primary difference between the 9-story model and the SDOF model is the participation of higher mode effects. The nature of this participation, however, cannot be easily apprehended, because it does not correlate directly with general observations of the ARS curves shown for the three ground motions in Figure 3.1. For instance, Figure 3.1 shows GM12 to have significant high frequency content, whereas Figure 4.1 shows the 9-story structure with the highest collapse resistance under GM12. This observation is consistent with comments made previously regarding such systems (Hines et al. 2009, 2011) that their strength and stiffness discontinuities cause some level of chaotic behavior that is sensitive not only to the shape of the response spectrum, but also the sequencing of pulses and other ground motion signal characteristics that are not typically considered in suite selection.

It can be seen in all the IDAS for the 9 story and one story braced frame that 1) the curves show weaving behavior and 2) there is one or more collapse areas in some of them. The same behavior was reported by Vamvatsikos and Cornell (2002). They discussed four different types of IDAS which are 1) Softening Case, 2) a bit of hardening, 3) Severe hardening, 4) Weaving behavior. The 4th behavior is very similar to OCBF IDA curves. It's interesting to be mentioned that they had all of these curves for a five- story braced frame and the responses ranging from a gradual degradation towards the collapse to a rapid twisting behavior which shows different levels of strain hardening. Though a gradual behavior looks more intuitive, but the hardening in the IDA curves was seen before in different works. Chopra also reported this behavior for simple bilinear elastic- perfectly plastic systems. In the extreme case, the structure may collapse in one or more scale factor and then be stable in a larger one (Figure 4.2). This behavior can be seen in Figure 4.3 which is the same as the IDA curve of the 9 story model for the GM4 and GM12.

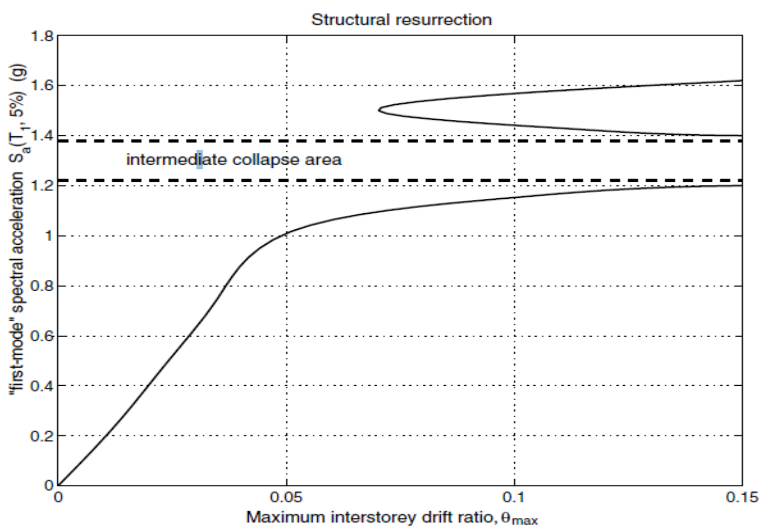

Figure 4.3. Structural resurrection on the IDA curve of a 3-story steel moment-resisting frame with fracturing connections

5. Ultimate Moment Prediction Models for Type 2 Connections

5.1. Scope

5.1.1. Motivation

An understanding of connection behavior is essential to design safe and effective reserve systems. A variety of connections have been tested experimentally since the 1930s, and multiple models have been developed to approximate the strength and stiffness relationships of these connections. However, most of these models focus on initial stiffness and stiffness degradation, while little has been determined about the strength of the connections at failure. Kishi and Chen (1990) developed models that include ultimate moment capacity predictions, but the theoretical basis of their equations does not provide insight into the physical behavior of the connection. It is the goal of this study to find a simple and intuitive model that can reasonably predict ultimate moment capacities of partially restrained connections, specifically Type 2. Type 2 (top and seat with double web angle) connections were chosen as the focus because of the large increase in moment capacity resulting from inexpensive and easy additions to simple connections.

The study estimates behavior of top and seat angle connections and double web angle connections separately before developing predictions for Type 2 connections. Figure 5.1 shows these three connection types.

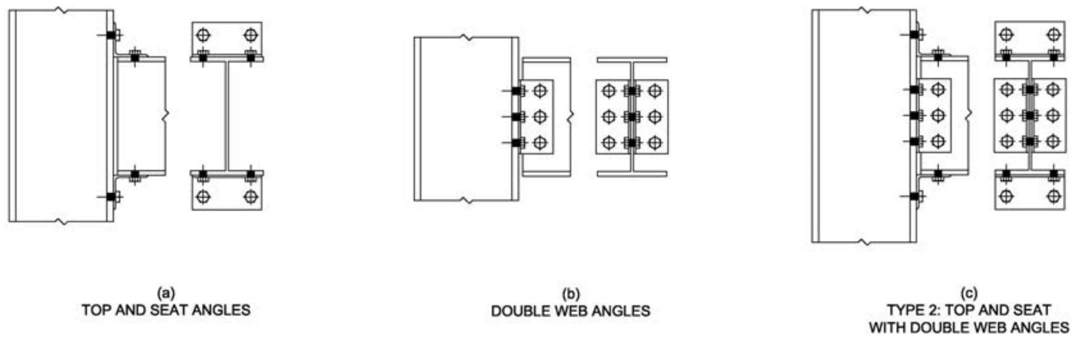

Figure 5.1. Connection types: (a) Top and seat angles; (b) Double web angles; (c) Type 2: top and seat with double web angles.

5.1.2. Process

The following sections discuss prediction models by Kishi and Chen (1990) (hereafter referred to as Chen's model) and Eurocode 3, Section 6.2.4. Chen's model is theoretically based in structural mechanics, using Tresca and Drucker-Prager yield criterion to determine ultimate resistance. Eurocode is the European Standard for calculating design resistances. Eurocode does not provide a method for calculating capacity of web angles; the study of double web angle and top and seat with double web angle connections include analyses only by Chen's model and the simplified model.

Additionally, the author proposes a simplified model based on physical behavior. Each model essentially follows a four-step process for determining the ultimate capacity of a connection:

1. Determine relevant connection parameters.

2. Calculate the internal flexural span.

3. Determine shear resistance.

4. Calculate ultimate moment capacity.

The models are used to predict behavior of connections that have previously been tested, and calculated results are compared to experimental.

The primary geometric parameter in predicting angle behavior in these models is the span between the two plastic hinges that are formed during angle yield, referred to as the internal flexural span, g2. The value of g2 is very important, as the prediction models are highly sensitive to slight differences in length. Ultimate shear and moment predictions are inversely related to g2. Each prediction model includes a different equation for g2 that greatly influences the models' results. Figure 5.2 compares g2 for the different models. In reality, the flexural span changes across the leg of the angle, as shown in Figure 5.3. The computed g2 is an approximated equivalent length.

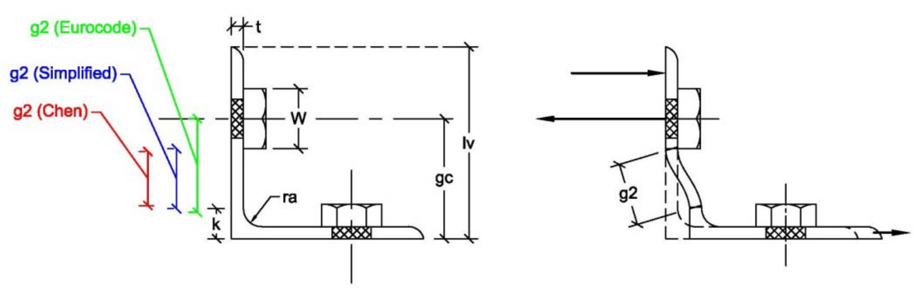

Figure 5.2. Internal flexural span, g_2.

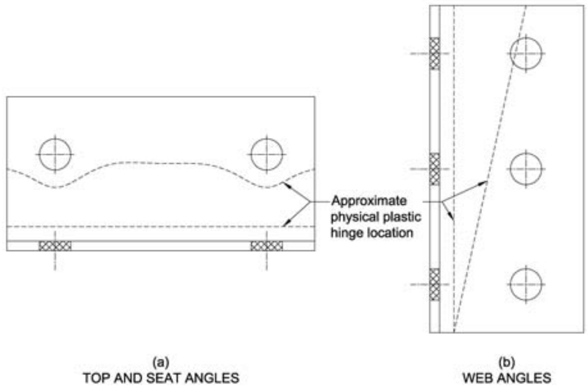

Figure 5.3. Approximation of g_2: (a) Top and seat angles; (b) Web angles

The aspect ratio of a connection is the ratio of the internal flexural span to the angle thickness. A high aspect ratio indicates an angle with a long, slender vertical leg, while a low aspect ratio indicates a short, stocky leg. This ratio is another parameter that is useful in predicting the behavior of a connection.

5.2. Top and Seat Angle Connections

Each prediction model calculates moment capacity differently but the relevant connection parameters remain the same. Figure 5.4 indicates the geometric properties represented by the following variables:

L_t = angle length

t_t = angle thickness

l_v = length of vertical leg of angle

k_t = angle fillet length

r_t = radius of angle fillet

g_{ct} = singular gage of angles (distance from angle heel to bolt centerline)

σ_y = angle yield stress

d = beam depth

Bolt: σ_u = ultimate stress

w = width of bolt head flats

d_b = diameter

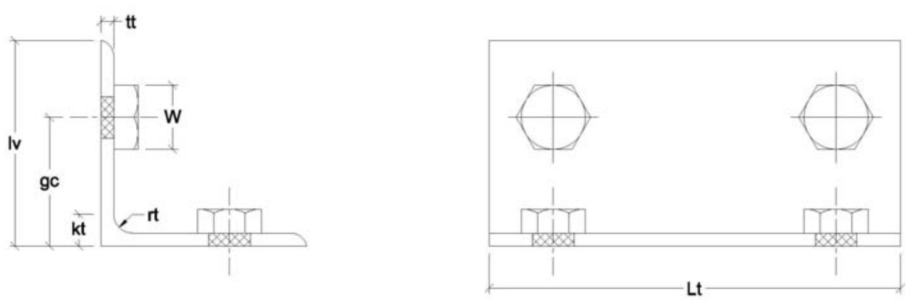

Figure 5.4. Top and seat angle connection geometry.

Chen's model permits different geometry for the top and seat angles. However, this discussion only considers top and seat angles with identical geometry to focus on computing resistance and simplify the models.

5.2.1. Chen's Model

Chen's model includes three components of the connection, illustrated in Figure

5.5, that contribute to moment resistance:

1. Plastic moment capacity of the seat angle, M_{os}
2. Plastic moment capacity of the secondary hinge in the top angle, M_p
3. Plastic shear resistance of the angle, V_p, multiplied by the distance to the center of rotation, d_2

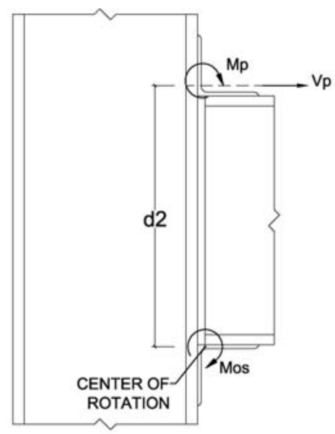

Figure 5.5. Chen's model: calculation of M_u.

Ultimate moment capacity, M_u, is the sum of these three components.

Appendix A.1 provides a more detailed discussion of Chen's model and example calculations.

5.2.2. Eurocode 3 Model

The analysis in Eurocode 3 Section 6.2.4 was developed for a T-stub under tension but allows for adjustments to similarly calculate the capacity of top and seat angles. Since the goal is prediction of actual behavior rather than design, safety factors (γ) provided in Eurocode have been excluded. Eurocode calculates shear capacity considering the following three modes of failure: angle yield; combination angle yield with bolt failure; and bolt failure. The lowest calculated shear capacity for a given connection is the predicted failure mode and capacity of the connection, V_p. M_u is the product of V_p and d_2, where d_2 is the sum of the beam depth, d, and singular gage, g_{ct}. See Figure 5.6.

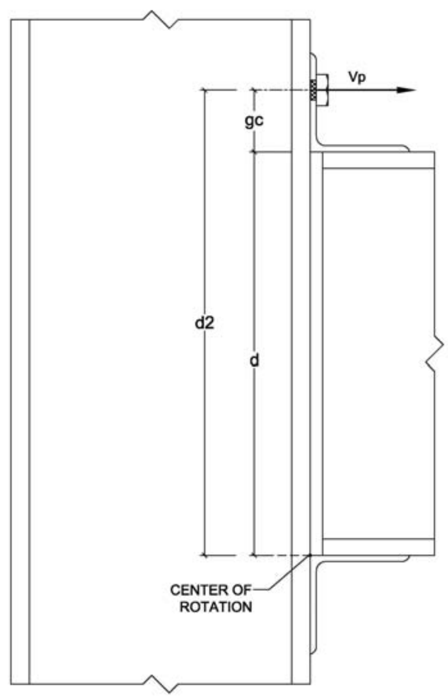

Figure 5.6. Eurocode and simplified models: calculation of M_u.

Further details and examples for the Eurocode model are included in Appendix A.2.

5.2.3. Simplified Model

The author developed the simplified model in an effort to predict ultimate moment capacity through an intuitive sequence of calculations that makes physical sense to a structural designer. The moment capacity of the angle provides the shear resistance, V_p, for the overall connection, and M_u is calculated similar to the Eurocode model by multiplying V_p by d_2 (Figure 5.6).

Refer to Appendix A.3 for a more comprehensive explanation and examples for the simplified method.

5.2.4. Comparison of Models and Experimental Data

Table 5.1 displays moment capacities as predicted by each model and compares them to experimental data by Kukreti et al (1999). Five specimens tested by Kukreti failed due to their bolts. These specimens were excluded from this analysis since Chen's model and the simplified model only account for angle yield.

The Eurocode model consistently under-predicts the moment capacity of the connections, with the lowest standard deviation of the three models. It may not be surprising that the Eurocode model is the most conservative, since it is intended as a guide for design rather than a precise prediction of connection behavior. Chen's model and the simplified model both over-predict the experimental data by approximately 10% on average, but the simplified model results are less precise, with a 0.42 standard deviation compared to Chen's model 0.20 standard deviation.

All three models tend to under-predict capacity for the connections with higher aspect ratios, as for Specimens 2 and 12. The opposite is somewhat true for a small aspect ratio too, as Specimen 11 has an aspect ratio of 0.71 and is well over-predicted by Chen's model and the simplified model. Eurocode under-predicts Specimen 11 but by much less than it under-predicts all the other connections. For Specimen 11, Eurocode predicts the combination failure mode of angle yield with bolt failure while Chen and simplified only consider angle yield.

Table 5.1. Top and seat angle moment capacity predictions.

Specimen	Aspect Ratio	Experimental**		Chen		Eurocode		Simplified (σ_y)	
	g_2* / t_t	M_{ux} (k-ft)	θ_u (rad)	M_{uc} (k-ft)	M_{uc}/M_{ux}	M_{ue} (k-ft)	M_{ue}/M_{ux}	M_{us} (k-ft)	M_{us}/M_{ux}
2	8.25	18	0.045	14	0.76	12	0.67	14	0.74
4	3.63	62	0.045	70	1.12	53	0.85	62	1.00
6	1.75	68	0.045	87	1.28	51	0.75	79	1.16
8	1.75	75	0.045	86	1.15	50	0.67	78	1.03
11	0.71	149	0.045	188	1.26	137	0.92	287	1.92
12	3.38	77	0.045	73	0.95	56	0.73	65	0.85
				Mean =	**1.09**		**0.77**		**1.12**
				Standard Deviation =	**0.20**		**0.10**		**0.42**

*g_2 in aspect ratio was calculated using the simplified model
**Experimental data from Kukreti et al (1999)

As mentioned in Section 5.1.2, the calculation of the internal flexural span g_2 has a large impact on the predictions of any model. Therefore, it is important to note the differences in each model's approach to the calculating g_2 based on their assumed plastic hinge locations. Note that in Eurocode 3, the length *m* is equivalent to what is referred to here as g_2. The equations for g_2 per model are as follows:

Chen's Model $g_2 = g_c - k_t - \frac{w}{2} - \frac{t_t}{2}$

Eurocode 3 Model $g_2 = g_c - t_t - 0.8r_a$

Simplified Model $g_2 = g_c - k_t - \frac{w}{2}$

All three models confine g_2 between the bolt centerline and angle fillet. (The Eurocode model includes a small portion of the fillet ($0.2r_a$) in g_2.) Chen's model and the simplified model subtract half the bolt head width that holds the angle leg against the column. The terms that include angle thickness in Chen's and the Eurocode model are approximations for the width of the plastic hinges. Overall, the Eurocode model generates the longest g_2 values, resulting in the lowest predictions, and Chen's model generates the shortest, which increase the predictions.

5.3. Double Web Angle Connections

The important connection parameters for web angle connections are listed below and illustrated in Figure 5.7.

L_p = angle length

t_a = angle thickness

k_a = angle fillet length

g_c = singular gage of angles

σ_y = angle yield stress

w = width of bolt head flats

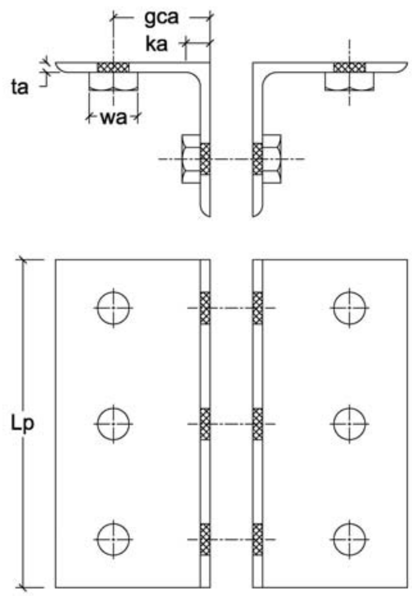

Figure 5.7. Double web angle connection geometry.

Because of a web angle's orientation, the connection shear distribution is not constant along the length of the angle. Figure 5.8 shows the deformed shape of double web angles, where it is obvious that the plastic hinge location varies.

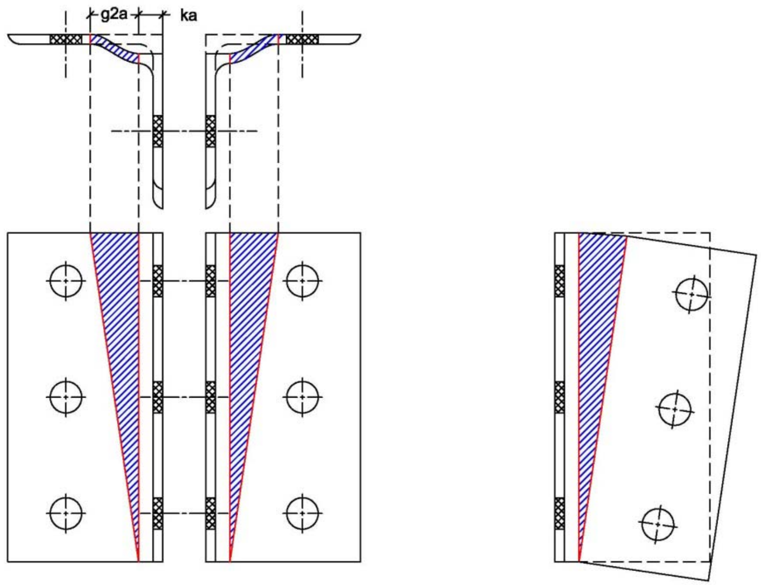

Figure 5.8. Deformed double web angle connection.

5.3.1. Chen's Model

For this connection type, Chen's model refers to the variable flexural span length as g_y rather than the constant g_2 discussed earlier. As seen in Figure 5.9, g_y is a linear function of the distance along the angle length, starting at the angle fillet k_a ($g_y = 0$) and ending at the bolt centerline ($g_y = g_c - k_a$). Appendix B.1 offers a more detailed explanation of the theory behind g_y, Chen's shear distribution, and the resulting applied shear force, V_a.

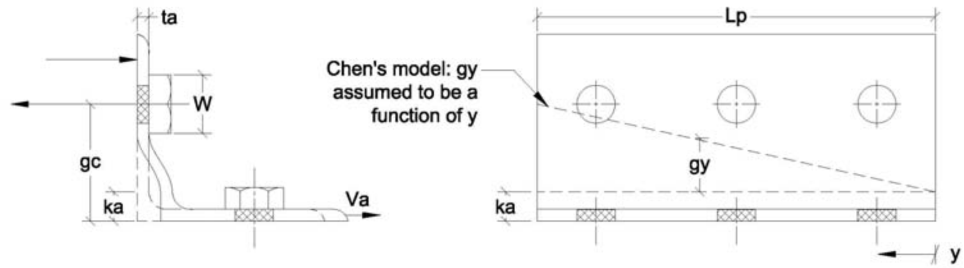

Figure 5.9. Internal flexural span for double web angles.

The center of rotation is located at the base of the web angle. The moment arm used to calculate M_u is the distance from the center of rotation to V_a, and is calculated based on the shear distribution geometry. Figure 5.10(a) shows the shear distribution and moment arm assumed by Chen's model.

5.3.2. Simplified Model

The simplified model calculates the internal flexural span g_2 and maximum shear capacity V_u the same as for top and seat angles. For the double web angles, however, the shear is distributed triangularly along the length, as shown in Figure 5.10(b).

The assumed triangular shape of distribution determines the resultant shear force V_a and length of moment arm. Similar to Chen's model, the center of rotation is located at the base of the angle. More detail on the simplified model is included in Appendix B.2.

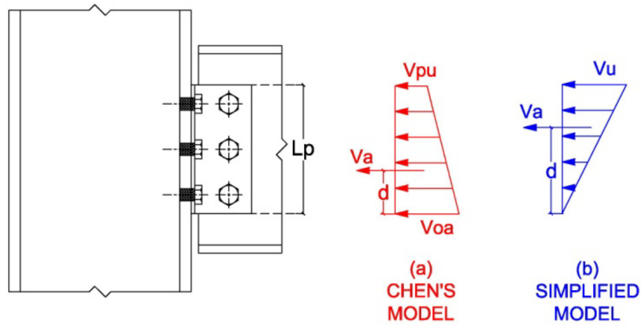

Figure 5.10. Assumed shear and moment resistance: (a) Chen's Model; (b) Simplified Model.

5.3.3. Comparison of Models and Experimental Data

Abolmaali et al (2003) conducted tests on double web angles. Five test specimens were excluded because they failed from web bearing rather than angle yield. Table 5.2 compares the remaining experimental data with capacity predictions by Chen's model and simplified model. Chen's model greatly over-predicts the moment capacity by an average 86%. The simplified model over-predicts as well but by the relatively low average of 11%, with the same standard deviation as Chen's.

Table 5.2. Double web angle moment capacity predictions.

Specimen	Aspect Ratio g_2^* / t_t	Experimental**		Chen		Simplified (σ_y)	
		M_{ux} (k-ft)	θ_u (rad)	M_{uc} (k-ft)	M_{uc}/M_{ux}	M_{us} (k-ft)	M_{us}/M_{ux}
DW-BB-1	3.21	9	0.050	16	1.76	7	0.81
DW-BB-2	3.21	15	0.050	27	1.76	13	0.81
DW-BB-4	3.21	24	0.050	56	2.31	26	1.06
DW-BB-5	1.81	45	0.050	89	1.99	63	1.40
DW-BB-6	1.81	14	0.050	26	1.86	18	1.31
DW-BB-7	1.81	29	0.050	45	1.58	32	1.11
DW-BB-12	1.72	69	0.045	120	1.74	85	1.24
				Mean =	**1.86**		**1.11**
				Standard Deviation =	**0.23**		**0.23**

*g_2 in aspect ratio was calculated using the simplified model

**Experimental data from Abolmaali et al (2003)

The simplified model has some advantages over Chen's model besides the numerical results. A distribution with the maximum force at the top of the angle for a downward rotation is much more intuitive than the inverted trapezoid distribution used in Chen's model. Triangular geometry is also simpler than trapezoidal to calculate forces and moment arms. Finally, Chen's model includes a fourth-order equation from the yield criterion, while the simplified method includes equations that can quickly be calculated by hand.

5.4. Type 2 Connections: Top and Seat Angles with Double Web Angles

The models for Type 2 connections are mostly a combination of the models of each individual connection type studied in sections 5.2 and 5.3, with a few exceptions that will be discussed per model. It is important to distinguish between the geometric and material parameters of the top and seat and double web angles. See Figure 5.11 for the relevant geometry of the connection, also listed below.

d = beam depth

Top, seat angles: L_t = angle length

t_t = angle thickness

k_t = angle fillet length

g_{ct} = singular gage of angles

σ_{yt} = angle yield stress

w_t = width of bolt head flats

Web angles: L_a = angle length

t_a = angle thickness

k_a = angle fillet length

g_{ca} = singular gage of angles

σ_{ya} = angle yield stress

w_a = width of bolt head flats

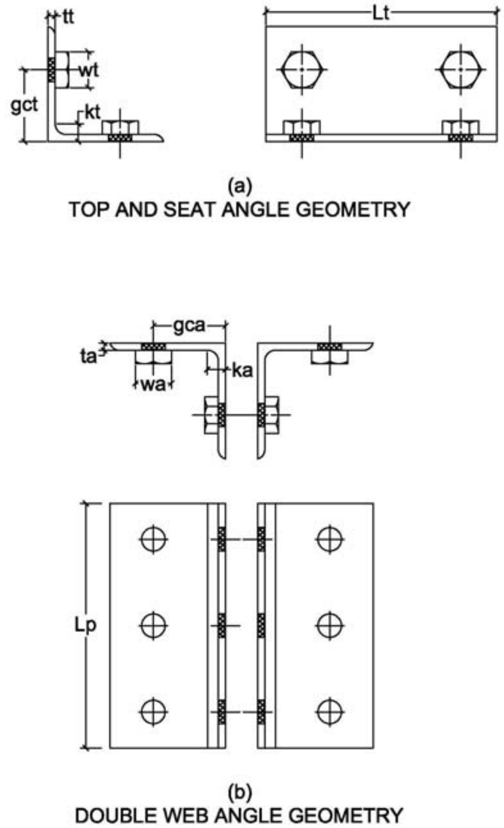

Figure 5.11. Top and seat angles with double web angles connection geometry.

Note that the variables are not always the same as Kishi and Chen (1990) use to describe the same parameters. The variables are named here to be consistent for both models.

5.4.1. Chen’s Model

Chen's model for Type 2 connections considers all four components of moment contribution from the models for top and seat angle connections and double web angle connections:

1. Plastic moment capacity of the seat angle, M_{os}

2. Plastic moment capacity of the secondary hinge in the top angle, M_{pt}

3. Plastic shear resistance of the top angle, V_{pt}, multiplied by the distance to the center of rotation, d_2

4. Plastic shear resistance of the double web angles, V_{pa}, multiplied by the distance to the center of rotation, d_3

Calculations for including top and seat angle moment resistance into Chen's model of the Type 2 connection do not change from section 5.1.1. The only difference from section 5.2.1 for including the double web angles is the shift in location of the center of rotation. The connection (including the web angles) rotates about a point halfway into the horizontal leg of the seat angle. Thus, the moment arm for V_{pa} is extended and the moment resistance increases. M_u is calculated by summing all of the resistance offered by top, seat, and both web angles. See Appendix C.1 for further investigation.

5.4.2. Simplified Model

As in Chen's model, the simplified model does not change in approach to top and seat angle capacity, and the double web angle capacity is changed by the shifted center of rotation. Not only does the moment arm change, but the amount of shear resisted by the angle increases as well. The reason for this is illustrated in Figure 5.12. The new shear distribution is truncated at the base of the web angle with a minimum shear value, V_1, and the result is a trapezoidal distribution. See Appendix C.2.

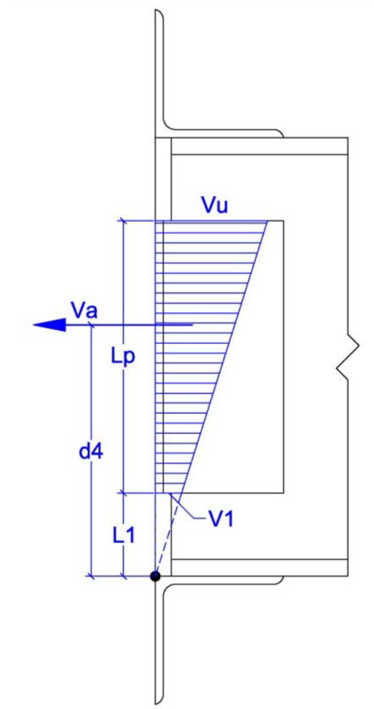

Figure 5.12. Shear distribution in web angles for Type 2 connections (simplified model).

5.4.3. Comparison of Models and Experimental Data

Table 5.3 compares predictions from Chen's model and the simplified model to experimental data from Azizinamini et al (1985). Chen's model appears to get extremely close predictions with an average 3% difference from experimental results. However, the level of confidence in the ability of Chen's model to predict the connection behavior may be tempered by the double web angle connection results in Table 5.2, where Chen's model over-predicted the moment capacity by up to 2.3 times the experimental data.

The results of the simplified model are consistent with those in Table 5.1 and Table 5.2, averaging just over 10% above the experimental moment capacity.

Table 5.3. Type 2 moment capacity predictions.

Specimen	Aspect Ratio g_2^*/t_t	Experimental**		Chen		Simplified (σ_y)	
		M_{ux} (k-ft)	θ_u (rad)	M_{uc} (k-ft)	M_{uc}/M_{ux}	M_{us} (k-ft)	M_{us}/M_{ux}
8S1	1.80	31	0.040	29	0.93	32	1.02
8S2	1.33	32	0.028	38	1.19	43	1.34
8S3	1.80	39	0.039	36	0.91	38	0.96
8S4	8.00	16	0.041	16	0.97	19	1.22
8S5	2.67	32	0.040	32	1.01	34	1.06
8S6	3.40	24	0.040	20	0.84	23	0.98
8S7	2.67	34	0.040	27	0.78	29	0.85
8S8	1.50	37	0.041	31	0.83	35	0.93
8S9	1.08	41	0.041	40	0.97	49	1.18
8S10	0.56	53	0.027	57	1.08	104	1.96
14S1	2.67	60	0.031	61	1.01	87	1.45
14S2	1.75	83	0.030	117	1.41	139	1.68
14S3	2.67	58	0.031	61	1.04	87	1.50
14S4	2.67	73	0.031	61	0.83	87	1.19
14S5	2.42	70	0.031	63	0.90	89	1.27
14S6	1.56	93	0.030	99	1.07	125	1.35
14S8	1.05	133	0.028	138	1.04	186	1.39
14S9	2.42	88	0.029	63	0.72	89	1.01
				Mean =	**0.97**		**1.24**
				Standard Deviation =	**0.16**		**0.29**

*g_2 in aspect ratio was calculated using the simplified model
**Experimental data from Azizinamini et al (1985)

5.5. Conclusions on Type 2 Study

From this preliminary study on predicting ultimate moment capacities of Type 2 connections, several conclusions are drawn for current and future consideration.

The prediction models offered by Kishi and Chen (1990) are theoretically based but do not always provide close or consistent results when compared with experimental test data. Predictions for each connection type require solving fourth-order equations that are not intuitive or efficient for practical use.

The simplified models proposed by the author do not claim to capture all of the complex behavior occurring within a yielding connection, but relies upon basic understanding and a transparent process to approximate ultimate moment capacity. The models need further refinement and over-predicted capacity by 10-15% the experimental results.

Investigating the Eurocode model was helpful as an additional comparison for top and seat angle capacities, but did not include an analysis for we angle connections. Eurocode was very conservative in its predictions, which might be attributed to its intended use in design. The basic theory behind the development of the Eurocode in the angle yield failure mode is similar to that of the simplified model.

A couple of issues have come up throughout the duration of this study.

1. None of the models currently account for strain hardening but depend on yield stress for predicting ultimate capacities.
2. There is not sufficient data on top and seat angle, double web angle, or Type 2 connections that were tested to failure to compare to the prediction models.

3. Some of the test data that has been used did not report certain dimensions, failure modes, or ultimate moments; these had to be assumed in order to complete the study.

Further work must be done before the moment capacities of these connections are able to be accurately predicted. Appendix D includes a comprehensive list of literature that has been compiled for this study, including data that has not yet been used to calibrate the prediction models. This study should be expanded to incorporate the additional data and consider other models once the literature has been reviewed. More experimental tests with complete data sets must be conducted, and the prediction models must be refined. However, it is clear that the types of connections discussed in this report all exhibit moment capacities to be considered in further development of reserve system design methodology.

6. Summary and Conclusions

The primary objective of this research is to develop confidence in collapse performance prediction of low-ductility chevron braced frames as discussed by Hines et al. (2009), who modeled these systems using Ruaumoko-2D (Carr 2004). The 2009 exposed stiffness and strength discontinuities of these systems that raised the question of whether consistent results could be expected between different software packages. For this reason, the current validation study was engaged in order to compare Ruaumoko results with results from large scale shake table tests and results from OpenSees (2006).

The best approach to develop confidence in modeling of collapse performance would be to compare analytical results with large scale experimental results. In the absence of experimental data related to the collapse performance of low-ductility braced frames, this study considered experimental work on a 4-story 1:8 scale moment frame at the State University of New York (SUNY) in Buffalo (Lignos 2008). This moment frame was tested to collapse, and therefore provided a good opportunity to calibrate OpenSees and Ruaomoko models for prediction of side sway collapse under dynamic and P-D effects. Results showed that there is an acceptable correlation between Ruaomoko, OpenSees and experimental data.

The object of the next portion of this study (Chapter 3) was to demonstrate that different software packages exhibit a high degree of consistency when used to model regular, ductile systems. Several simple models were considered: 1) Cantilever, 2) 1-story moment resistant frame (MRF), and 3) 1-story eccentric braced frame (EBF). The IDA and displacement time history comparison for all ductile systems showed a good match between OpenSees and Ruaomoko. These results coupled with the NEES Buffalo Frame Study indicated that: 1) it is possible to model the nonlinear behavior of ductile systems with high confidence and 2) there is a good match between maximum displacements for all models but the residual displacements can vary significantly. Note that Yazgan and Dazio (ETH Workshop, 2006) drew similar conclusions from comparative studies of reinforced concrete structural walls modeled with OpenSees and Ruaumoko, and indicated that it may be possible to address this issue

Based on these promising results, a one story chevron braced frame with reserve system was modeled in OpenSees and Ruaomoko. There were three main differences between the results of this system compared with ductile systems which were:

1) The IDA curve of this system showed weaving behavior while ductile systems show softening or hardening behavior.

2) The correlation of IDA curves and time history displacement between OpenSees and Ruaomoko for this system was not as good as for ductile systems.

3) There were some convergence problems in the model obscuring whether non-convergence represented physical collapse or some other numerical instability.

These results indicated that differences between OpenSees and Ruaomoko could stem from the characteristic of brittle systems which is related to the brace fracture model and sudden change of stiffness and strength of the systems. For these reasons, it is important to exercise caution when modeling such systems, and it is advisable to report results from more than one modeling approach or software package. Ultimately, it will be very important to calibrate low-ductility braced frame models against experimental data.

In spite of the persisting uncertainties related to modeling these systems, it is still possible to observe significant correlation between reserve capacity and collapse resistance. Doubling the reserve capacity for the one story low-ductility braced frame in Chapter 3 increased the collapse capacity significantly. Conversely, cutting the reserve capacity in half reduced collapse capacity by more than a factor of 2.

The 9-story model was created in both software packages and the IDA curves were compared. This study only considered the 9-story R3 model so far. Results indicated that like one story braced frame model, the IDA curves showed weaving behavior and there were some convergence problems in the model.

Finally, some of the basics of partially restrained connections were discussed based on a literature review of bolted double web angle connections and bolted top and seat angle connections used for Type II construction. This discussion emphasized the need for analytical models that can reliably predict the ultimate moment capacity of particular connections. Such a model could facilitate the design of reserve systems based on very simple considerations. Previous researchers have investigated such connections with respect to their elastic performance under wind loads, and paid comparatively little attention to the moment-rotation performance of these connections up to the point of fracture. Based on this observation, it is recommended to develop an experimental and analytical program on these connections that focuses on their ultimate strength and deformation capacities.

Future work will include the following tasks:

- Further literature review of modeling issues, collapse behavior of building structures, and experimental performance of PR connections.
- Experimental and analytical program to understand ultimate strength and deformation capacities of PR connections in terms of simple, physical models.
- Design a 9-story low ductility chevron braced frame with partially restrained connections. This system will be designed with the assumption that moment frames will take all the earthquake loads and the braced frames are for drift control.
- Model this system in OpenSees and Ruaomoko and study the collapse behavior.
- Investigate the possibility of incorporating IDA results from all scale factors into reliability-based collapse assessment methods. Currently, only the scale

factor associated with collapse is used for collapse performance assessment, and behavior at scale factors below the collapse level are ignored in the formal assessment procedure.

- Model braces such that they don’t fracture at the same time, and investigate other possible refinements to the system models, such as base plates, column splices, etc.

References:

Abolmaali, A., A.R. Kukreti, & H. Razavi. (2003). Hysteresis behavior of semi-rigid double web angle steel connections. Journal of Constructional Steel Research, 59:1057-1082.

Carr, A.J. (2004), *Ruaumoko Manual Volumes 1 & 2*, University of Canterbury, Christchurch, New Zealand, 333 pp.

Chen, W.F. (2000). Practical Analysis for Semi-Rigid Frame Design. World Scientific, Singapore.

Disque, R.O. (1976) Type 2 Construction with wind moment connections: a return to simplicity, AISC.

Eurocode 3: Design of steel structures. Parts 1-8: Design of joints.

FEMA 355-D, (2000) State of the Art Report on Connection Performance. Federal Emergency of Management Agency.

Geschwinder, L.F. and Disque, R.O. (2005) “Flexible Moment Connections for Unbraced Frames Subject to Lateral Forces—A Return to Simplicity,” AISC Engineering Journal, Second Quarter, pp. 99-112.

Hines, E.M., Appel, M.E. and Cheever, P.J. (2009) “Collapse Performance of Low-Ductility Chevron Braced Steel Frames in Moderate Seismic Regions,” *AISC Engineering Journal*, 3rd Quarter, pp. 149-180.

Hines, E.M. and Fahnestock, L.A. (2010) “Design Philosophy for Steel Structures in Moderate Seismic Regions,” *9th US National and 10th Canadian Conference on Earthquake Engineering*, EERI/CAEE, Toronto, Canada, July 25-29.

Hines, E.M., Baise, L.G. and Swift, S.S. (2011) “Ground Motion Suite Selection for Eastern North America,” *ASCE Journal of Structural Engineering*, 137(3), March, pp. 358-366.

Kishi, N., & W.F. Chen. (1990). Moment-rotation relations of semirigid connections with angles. J. Struct. Eng., 116(7):1813-1834.

Kukreti, A.R., & A.S. Abolmaali. (1999). Moment rotation hysteresis behavior of top and seat angle steel frame connections. J. Struct. Eng., 125(8):810-820.

Lignos, D.G. (2008) Sidesway Collapse of Deteriorating Structural Systems under Seismic Excitations, Ph.D. Dissertation, Department of Civil and Environmental Engineering, Stanford University, 457 pp.

Lignos, D.G., Krawinkler, H. and Whittaker, A.S. (2010) “Prediction and validation of sidesway collapse of two scale models of a 4-story steel moment frame,” *Earthquake Engineering and Structural Dynamics*, Wiley Online Library, DOI: 10.1002/eqe.

Rodgers, J.E., Mahin,S.A.,(2004) Effects of Hysteretic Deterioration on Seismic Response of Steel Moment Frames, *Paper No.1581. 13th World conference on Earthquake Engineering, Vancouver, B.C.,Canada.*

Sorabella, S. (2006) *Ground Motion Selection for Boston, Massachusetts*, Masters Thesis, Department of Civil and Environmental Engineering, Tufts University, Medford, Massachusetts, 213 pp.

Uang, C. M. and Bertero, V. V. (1986) Earthquake Simulation Tests and Associated Studies of a 0.3-Scale Model of a Six-Story Concentrically Braced Steel Structure, *Report No. UCB/EERC-86/10*, University of California, Berkeley, 363 pp.

Vamvastikos, D. and Cornell, C.A. (2002) " Incremental Dynamic Analysis," *Earthquake Engineering and Structural Dynamic.*

Whittaker, A. S., Uang. C. M., and Bertero, V. V. (1990) An Experimental Study of the Behavior of Dual Steel Systems, *Report No. UCB/EERC-88/14*, University of California, Berkeley.

Appendix A

Appendix A describes three models used for the prediction of ultimate moment capacity for top and seat angle connections.

A.1. Chen's Model

Calculate internal flexural span.

Chen's model assumes plastic hinges form at the top of the angle fillet and at the edge of the bolt heads. Additionally, the width of each plastic hinge line is assumed to equal half the thickness of the angles. These assumptions are accounted for in Chen's model equation for g_{2t}.

$$g_{2t} = g_{ct} - k_t - \frac{w_t}{2} - \frac{t_t}{2} \qquad \text{(in)}$$

Determine shear resistance.

Maximum plastic shear resistance, V_{ot}, from Tresca's yield criterion:

$$V_{ot} = \frac{L_t t_t \sigma_{yt}}{2} \qquad \text{(k)}$$

Plastic shear resistance of top angle, V_{pt}

$$\left(\frac{V_{pt}}{V_{ot}}\right)^4 + \frac{g_{2t}}{t_t}\left(\frac{V_{pt}}{V_{ot}}\right) - 1 = 0$$

Solve the fourth order equation for V_{pt} (k)

This fourth order equation derives from the Drucker-Prager yield criterion and the relationship between the pure plastic flexural capacity and shear capacity of the angle as described by Tresca's yield criterion. Due to the combination of flexural and shear demand on the angle, the plastic shear resistance of the angle is reduced from a maximum value, V_{ot} (pure shear demand), to a lower value, V_{pt} (combined shear and flexure demand).

Calculate ultimate moment capacity.

Plastic moment capacity of secondary hinge in top angle, M_{pt}

$$M_{pt} = \frac{V_{pt} g_{2t}}{2} \qquad \text{(k-in)}$$

Plastic moment capacity of seat angle, M_{os}

$$M_{os} = Z_t \sigma_y = \frac{L_t {t_t}^2 \sigma_y}{4} \qquad \text{(k-in)}$$

Since the vertical leg of the seat angle is flat against the column when the connection is subjected to positive bending, the only deformation in the angle will be flexural bending of the horizontal leg. Thus, the moment capacity of this angle leg, M_{os}, is calculated as the pure plastic bending moment capacity of the angle section.

Ultimate moment of connection, M_u

$$M_u = M_{pt} + M_{os} + V_{pt} d_2 \qquad \text{(k-in)}$$

where $d_2 = d + \frac{t_t}{2} + k_t$ (in)

The ultimate moment capacity is equal to the sum of the three moment contributions: M_{pt}, M_{os}, and $V_{pt}d_2$. These three contributions are derived from the moment resistance of the top angle, the moment resistance of the seat angle, and the shear resistance of the top angle, respectively. It should be noted that the majority of M_u is a result of $V_{pt}d_2$.

The variable d_2 represents the distance from the center of rotation to the line of action of V_{pt}. Chen's model assumes that the center of rotation is located half the thickness of the seat angle below the bottom flange of the beam and that the line of action of V_{pt} occurs at the top of the top angle fillet.

Example A.1

Determine relevant connection parameters.

Connection geometry from Kukreti et al (1999) - Specimen 6

L_t = 8.0 in

t_t = 0.5 in

k_t = 1.0 in

g_{ct} = 2.5 in

σ_{yt} = 51 ksi

w_t = 1.25 in

d = 13.7 in

Calculate internal flexural span.

$$g_{2t} = g_{ct} - k_t - \frac{\mathrm{w_t}}{2} - \frac{\mathrm{t_t}}{2} = 2.5 \text{ in} - 1.0 \text{ in} - \frac{1.25 \text{ in}}{2} - \frac{0.5 \text{ in}}{2} = 0.625 \text{ in}$$

Determine shear resistance.

$$V_{ot} = \frac{L_t t_t \sigma_{yt}}{2} = \frac{(8 \text{ in})(0.5 \text{ in})(51 \text{ ksi})}{2} = 102 \text{ k}$$

$$\left(\frac{V_{pt}}{V_{ot}}\right)^4 + \frac{g_{2t}}{t_t}\left(\frac{V_{pt}}{V_{ot}}\right) - 1 = \left(\frac{V_{pt}}{102 \text{ k}}\right)^4 + \frac{0.625 \text{ in}}{0.5 \text{ in}}\left(\frac{V_{pt}}{102 \text{ k}}\right) - 1 = 0$$

Solve fourth order equation → V_{pt} = 66.7 k

Calculate ultimate moment capacity.

$$M_{pt} = \frac{V_{pt} g_{2t}}{2} = \frac{(67 \text{ k})(0.625 \text{ in})}{2} = 20.9 \text{ k-in} = 1.74 \text{ k-ft}$$

$$M_{os} = \frac{L_t {t_t}^2 \sigma_{yt}}{4} = \frac{(8 \text{ in})(0.5 \text{ in})^2(51 \text{ ksi})}{4} = 25.5 \text{ k-in} = 2.13 \text{ k-ft}$$

$$d_2 = d + \frac{t_t}{2} + k_t = 13.7 \text{ in} + \frac{0.5 \text{ in}}{2} + 1.0 \text{ in} = 15.0 \text{ in}$$

$$V_{pt} d_2 = (66.7 \text{ k})(15 \text{ in}) = 1001 \text{ k-in} = 83.4 \text{ k-ft}$$

$$M_u = M_{pt} + M_{os} + V_{pt} d_2 = 1.74 \text{ k-ft} + 2.13 \text{ k-ft} + 83.4 \text{ k-ft} = \boxed{87.3 \text{ k-ft}}$$

A.2. Eurocode Model

Calculate internal flexural span.

In this model, it is assumed that plastic hinges form at 80% of the height of the top angle fillet and at the centerline of the bolt holes, yielding the following equation for g_{2t}:

$$g_{2t} = g_{ct} - t_t - 0.8 r_t \qquad \text{(in)}$$

Note that Eurocode uses the variable *m* to describe the length that is referred to here as g_{2t}.

Determine shear resistance.

Mode 1: Angle yield

Eurocode provides two methods for calculating Mode 1. Method 1 considers the force to be applied along the bolt centerline, and Method 2 applies a uniformly distributed load across the bolt head. Only Method 2 is considered for this study as the results are more accurate.

Plastic moment resistance of top angles, M_{pt}

$$M_{pt} = Z_t \sigma_{yt} = \frac{L_{eff} {t_t}^2 \sigma_{yt}}{4} \qquad \text{(k-in)}$$

where $L_{eff} = \frac{L_t}{2}$ (in)

L_{eff} is the adjusted angle length for the equivalent T-stub analysis.

Plastic shear resistance, V_{pt}

$$V_{pt} = \frac{(8n - 2e_w)M_{pt}}{2g_{2t}n - e_w(g_{2t} + n)} \quad \text{(k)}$$

where $e_w = \frac{w_t}{4}$ (in)

$$n = l_{vt} - g_{ct} \leq 1.25 g_{2t} \quad \text{(in)}$$

Mode 2: Angle yield with bolt failure

Tension resistance of a single bolt, F_t

$$F_t = k_2 \sigma_u A_s \quad \text{(k)}$$

where k_2 = 0.9 (Eurocode Table 3.4)

A_s = cross-sectional area of bolt (in^2)

Plastic shear resistance, V_{pt}

$$V_{pt} = \frac{2M_{pt} + n\sum F_t}{g_{2t} + n} \quad \text{(k)}$$

Mode 3: Bolt failure

Plastic shear resistance, V_{pt}

$$V_{pt} = \sum F_t \qquad \text{(k)}$$

Calculate ultimate moment capacity.

Ultimate moment of connection, M_u

$$M_u = dV_{pt} \qquad \text{(k-in)}$$

Example A.2

Determine relevant connection parameters.

Connection geometry from Kukreti et al (1999) - Specimen 6

L_t = 8.0 in

l_{vt} = 4.0 in

t_t = 0.5 in

k_t = 1.0 in

r_t = 0.50 in

g_{ct} = 2.5 in

σ_{yt} = 51 ksi

d = 13.7 in

Bolts: d_b = 0.75 in

w_t = 1.25 in

σ_u = 120 ksi

Calculate internal flexural span.

$$g_{2t} = g_{ct} - t_t - 0.8r_t = 2.5 \text{ in} - 0.5 \text{ in} - 0.8(0.5 \text{ in}) = 1.6 \text{ in}$$

Determine shear resistance.

$$L_{eff} = \frac{L_t}{2} = \frac{8 \text{ in}}{2} = 4 \text{ in}$$

$$M_{pt} = \frac{L_{eff} {t_t}^2 \sigma_{yt}}{4} = \frac{(4 \text{ in})(0.5 \text{ in})^2 (51 \text{ ksi})}{4} = 12.8 \text{ k-in}$$

$$e_w = \frac{w_t}{4} = \frac{1.25 \text{ in}}{4} = 0.313 \text{ in}$$

$$n = l_{vt} - g_{ct} = 4.0 \text{ in} - 2.5 \text{ in} = 1.5 \text{ in}$$

Mode 1: Angle yield

$$V_{pt} = \frac{(8n - 2e_w)M_{pt}}{2g_{2t}n - e_w(g_{2t} + n)} = \frac{(8(1.5 \text{ in}) - 2(0.313 \text{ in}))12.8 \text{ k-in}}{2(1.6 \text{ in})(1.5 \text{ in}) - (0.313 \text{ in})(1.6 \text{ in} + 1.5 \text{ in})} = 38 \text{ k}$$

Mode 2: Angle yield with bolt failure

$$k_2 = 0.9$$

$$A_s = \frac{\pi {d_b}^2}{4} = \frac{\pi (0.75 \text{ in})^2}{4} = 0.442 \text{ in}$$

$$F_t = k_2 \sigma_u A_s = 0.9(120 \text{ ksi})(0.442 \text{ in}) = 47.7 \text{ k}$$

$$\sum F_t = 2(47.7 \text{ k}) = 95.4 \text{ k}$$

$$V_{pt} = \frac{2M_{pt}+n\sum F_t}{g_{2t}+n} = \frac{2(12.8\text{ k-in})+(1.5\text{ in})(95.4\text{ k})}{(1.6\text{ in})+(1.5\text{ in})} = 54.4\text{ k}$$

Mode 3: Bolt failure

$$V_{pt} = \sum F_t = 95.4\text{ k}$$

Minimum of Modes 1, 2 and 3: $V_{pt} = 38$ k.

→ Predicted failure mode is angle yielding.

Calculate ultimate moment capacity.

$$M_u = dV_{pt} = (13.7\text{ in})(38\text{ k}) = 521\text{ k-in} = \boxed{43.4\text{ k-ft}}$$

A.3. Simplified Model

Calculate internal flexural span.

In this model, it is assumed that plastic hinges form at the top of the angle fillet and at the edge of the bolt heads, yielding the following equation for g_{2t}:

$$g_{2t} = g_{ct} - k_t - \frac{w_t}{2} \qquad \text{(in)}$$

Determine shear resistance.

The maximum moment capacity of the angle in pure flexure is equal to the plastic section modulus multiplied by the yield stress of the angle.

Maximum plastic moment resistance, M_{pt}

$$M_{pt} = Z_t \sigma_{yt} = \frac{L_t {t_t}^2 \sigma_{yt}}{4} \qquad \text{(k-in)}$$

The maximum shear resistance of the angles can be calculated by assuming fixity at both plastic hinges. Under this assumption, the angle leg experiences perfect double bending and the shear span is exactly half the flexural span as shown in Figure A.1. The maximum shear resistance is equal to the maximum moment divided by the shear span.

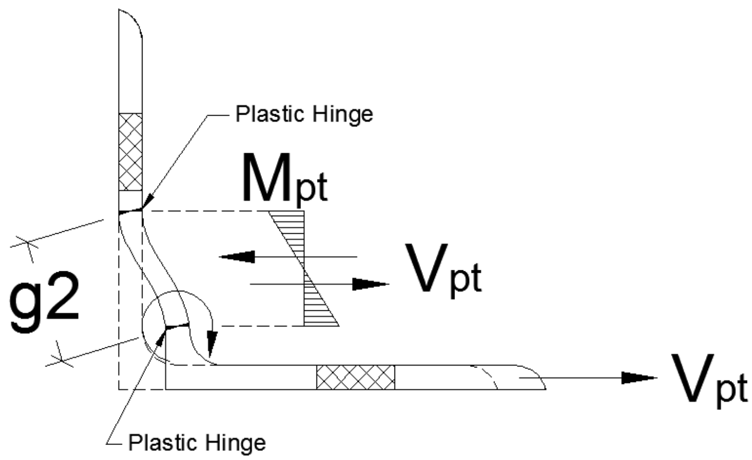

Figure A.1. Maximum shear resistance in angle leg assuming double bending.

Maximum plastic shear resistance, V_{pt}

$$V_{pt} = \frac{M_{pt}}{(g_{2t}/2)} \qquad \text{(k)}$$

Calculate ultimate moment capacity.

Figure A.2 illustrates d_2, which is the moment arm for the ultimate moment capacity of the connection. This moment arm spans between the center of rotation and the shear resistance force V_{pt}, which acts at the centerline of the bolt holes in the top angle; therefore, d_2 is calculated as:

$$d_2 = d + g_{ct} \qquad \text{(in)}$$

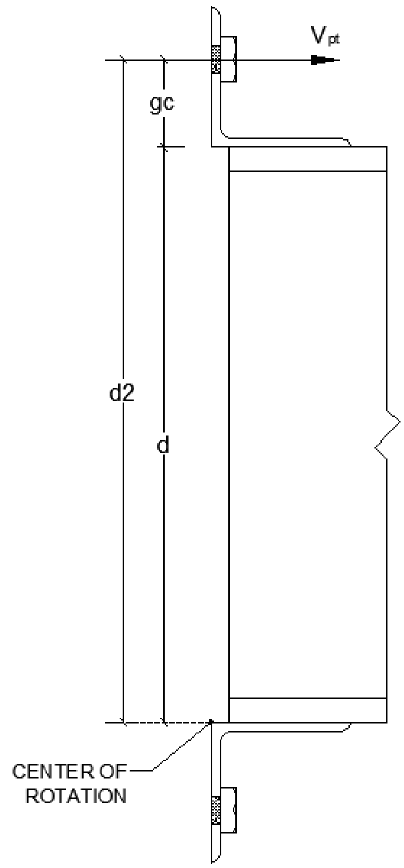

Figure A.2. Moment arm of maximum shear resistance of top and seat angle connection (simplified model).

Ultimate moment capacity of the connection, M_u

$$M_u = V_{pt} d_2 \qquad \text{(k-in)}$$

Example A.3

Determine relevant connection parameters.

Connection geometry from Kukreti et al (1999) – Specimen 6

$L_t = 8.0$ in

$t_t = 0.5$ in

$k_t = 1.0$ in

$g_{ct} = 2.5$ in

$\sigma_{yt} = 51$ ksi

$w_t = 1.25$ in

$d = 13.7$ in

Calculate internal flexural span.

$$g_{2t} = g_{ct} - k_t - \frac{\mathrm{w_t}}{2} = 2.5\text{ in} - 1.0\text{ in} - \frac{1.25\text{ in}}{2} = 0.875\text{ in}$$

Determine shear resistance.

$$M_{pt} = \frac{L_t \mathrm{t_t}^2 \sigma_{\mathrm{yt}}}{4} = \frac{(8.0\text{ in})(0.5\text{ in}^2)(51\text{ ksi})}{4} = 25.5\text{ k-in}$$

$$V_{pt} = \frac{M_{pt}}{(g_{2t}/2)} = \frac{(25.5\text{ k-in})}{(0.875\text{ in}/2)} = 58.3\text{ k}$$

Calculate ultimate moment capacity.

$$d_2 = d + g_{ct} = (13.7\text{ in}) + (2.5\text{ in}) = 16.2\text{ in}$$

$$M_u = V_{pt} d_2 = (58.3 \text{ k})(16.2 \text{ in}) = 944 \text{ k-in} = \boxed{78.7 \text{ k-ft}}$$

Example A.4

Determine relevant connection parameters.

Connection geometry from Kukreti et al (1999) – Specimen 2

L_t = 8.0 in

t_t = 0.375 in

k_t = 0.875 in

g_{ct} = 4.5 in

σ_{yt} = 49 ksi

w_t = 1.0625 in

d = 13.7 in

Calculate internal flexural span.

$$g_{2t} = g_{ct} - k_t - \frac{w_t}{2} = 4.5 \text{ in} - 0.875 \text{ in} - \frac{1.0625 \text{ in}}{2} = 3.09 \text{ in}$$

Determine shear resistance.

$$M_{pt} = \frac{L_t \mathrm{t_t}^2 \sigma_{\mathrm{yt}}}{4} = \frac{(8.0 \text{ in})(0.375 \text{ in}^2)(49 \text{ ksi})}{4} = 13.8 \text{ k-in}$$

$$V_{pt} = \frac{M_{pt}}{(g_{2t}/2)} = \frac{(13.8 \text{ k-in})}{(3.09 \text{ in}/2)} = 8.92 \text{ k}$$

Calculate ultimate moment capacity.

$$d_2 = d + g_{ct} = (13.7 \text{ in}) + (4.5 \text{ in}) = 18.2 \text{ in}$$

$$M_u = V_{pt} d_2 = (8.92 \text{ k})(18.2 \text{ in}) = 162 \text{ k-in} = \boxed{13.5 \text{ k-ft}}$$

Appendix B

Appendix B describes two models used for the prediction of ultimate moment capacity for double web angle connections.

B.1. Chen's Model

Calculate internal flexural span.

This model uses the variable g_y (instead of g_{2a}) to represent the length of the internal flexural span of the angles. In the top and seat angle connection prediction models discussed in Appendix A, the internal flexural span is approximated as constant along the length of the angles since the shear demand and deformed shape are constant along the length.

Due to the vertical orientation of the double web angles, however, the shear demand and deformed shape of these angles are not constant along the length of the angles. Thus, for the double web angle model, Chen assumes g_y is a function of y, the height along the angles. More specifically, Chen assumes:

$$g_y = (g_{ca} - k_a)\frac{y}{L_a} \qquad \text{(in)}$$

Chen's assumption for g_y is illustrated with respect to the deformed shape of a double web angle connection in Figure B.1. Clearly the assumption of a linearly varying shear span is consistent with the physical deformed shape of the double web angles.

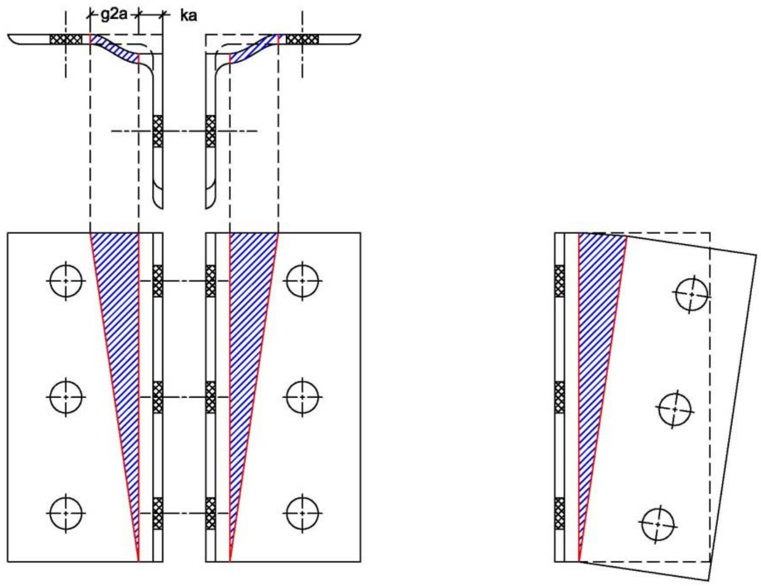

Figure B.1. Deformed double web angle connection.

Determine shear resistance.

Similar to Chen's model for top and seat angle connections, Chen's model for double web angle connections uses Tresca's yield criterion to determine internal shear and moment capacity of the angles. The major difference between the two models is that the internal flexural span is assumed to be constant along the length of the angles in the top and seat angle model, whereas in the double web angle model, it is not. This difference is shown in Figure B.2.

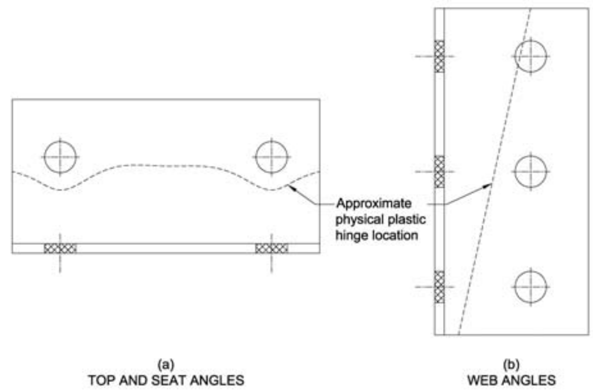

Figure B.2. Approximation of g_2: (a) Top and seat angles; (b) Web angles

As a result of the linearly varying flexural span assumption, the fourth order equation in this model will produce a parabolic distribution of shear resistance, V_y, along the angles. Chen, however, makes the simplifying assumption that this distribution is linear. Since $g_y(y = 0) = 0$, the fourth order equation yields $V_y = V_{oa}$ when $y = 0$ (at the bottom of the angles). Additionally, the assumption of a linear shear resistance distribution requires only one more value of V_y to be calculated in order to determine the shear resistance distribution along the angles. More specifically, V_y must be calculated when $y = L_a$ (the top of the angles) where $g_y = g_{ca} - k_a$.

Maximum plastic shear resistance, V_{oa}

$$V_{oa} = \frac{L_a t_a \sigma_{ya}}{2} \qquad \text{(k/in)}$$

Note that V_{pu} is the variable that has been assigned to the value of V_y when the fourth order equation is evaluated for V_y at $g_y = g_{ca} - k_a$.

Minimum plastic shear resistance ($g_y = g_{ca} - k_a$), V_{pu}

$$\left(\frac{V_y}{V_{oa}}\right)^4 + \frac{g_y}{t_a}\left(\frac{V_y}{V_{oa}}\right) - 1 = 0$$

Solve the fourth order equation for V_{pu} (k/in)

Total shear resistance of each web angle, V_a

$$V_a = \frac{L_a(V_{pu}+V_{oa})}{2} \qquad \text{(k)}$$

The resulting shear resistance in each web angle is an inverted trapezoidal distribution with a maximum value V_{oa} at the bottom of the angles and a minimum value V_{pu} at the top of the angles. The total shear resistance of each web, V_a, is equal to the area of this trapezoidal distribution. This distribution is shown in Figure B.3.

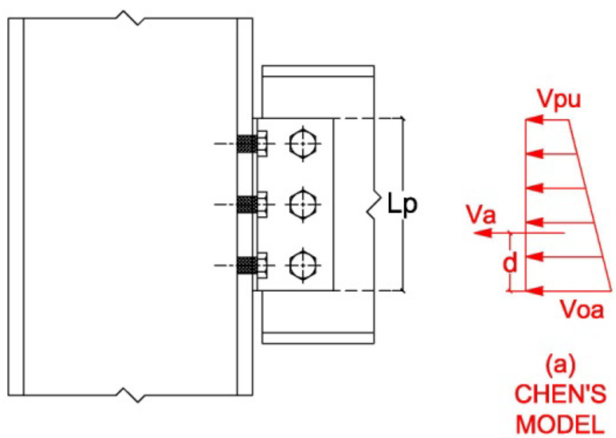

Figure B.3. Assumed shear resistance of double web angles (Chen’s Model)

Calculate ultimate moment capacity.

The distance between the assumed center of rotation (the bottom of the angles) and the centroid of the shear resistance distribution, d_3, is the moment arm over which V_a acts. The ultimate moment capacity for a single web angle is the product of V_a and d_3; M_u of the entire double angle connection is twice the resistance of a single angle.

$$d_3 = \frac{L_p(2V_{pu}+V_{oa})}{3(V_{pu}+V_{oa})} \qquad \text{(in)}$$

$$M_u = 2V_a d_3 = \frac{(2V_{pu}+V_{oa})}{3} {L_a}^2 \qquad \text{(k-in)}$$

Example B.1

Determine relevant connection parameters.

Connection geometry from Abolmaali et al (2003) - Specimen DW-BB-4

L_a = 14.5 in

t_a = 0.25 in

k_a = 0.625 in

g_{ca} = 2.1 in

σ_{ya} = 57 ksi

$w_a = 1.25$ in

Calculate internal flexural span.

$$g_y = g_{ca} - k_a = 2.1 \text{ in} - 0.625 \text{ in} = 1.475 \text{ in}$$

Determine shear resistance.

$$V_{oa} = \frac{L_a t_a \sigma_{ya}}{2} = \frac{(14.5 \text{ in})(0.25 \text{ in})(57.0 \text{ ksi})}{2} = 7.125 \text{ k/in}$$

$$\left(\frac{V_{pu}}{V_{oa}}\right)^4 + \frac{g_y}{t_a}\left(\frac{V_{pu}}{V_{oa}}\right) - 1 = \left(\frac{V_{pu}}{7.125 \text{ k/in}}\right)^4 + \frac{1.475 \text{ in}}{0.25 \text{ in}}\left(\frac{V_{pu}}{7.125 \text{ k/in}}\right) - 1 = 0$$

Solve fourth order equation → $V_{pu} = 1.2$ k/in

$$V_a = \frac{L_a(V_{pu} + V_{oa})}{2} = \frac{(14.5 \text{ in})(1.2 \text{ k/in} + 7.125 \text{ k/in})}{2} = 60.4 \text{ k}$$

Calculate ultimate moment capacity.

$$M_u = \frac{(2V_{pu} + V_{oa})}{3} L_a{}^2 = \frac{(2*1.2 \text{ k/in} + 7.125 \text{ k/in})}{3} (14.5 \text{ in})^2 = 668 \text{ k-in} = \boxed{55.6 \text{ k-ft}}$$

B.2. Simplified Model

Calculate internal flexural span.

In this model, it is assumed that plastic hinges form at the top of the angle fillet and at the edge of the bolt heads, yielding the following equation for g_{2a}:

$$g_{2a} = g_{ca} - k_a - \frac{w_a}{2} \qquad \text{(in)}$$

Note that in the simplified models, the equation for g_2 does not change between top and seat angle connections and double web angle connections.

Determine shear resistance.

Maximum plastic moment resistance, M_{pa} (under pure flexure)

$$M_{pa} = Z_a \sigma_{ya} = \frac{{t_a}^2 \sigma_{ya}}{4} \qquad \text{(k-in/in)}$$

Maximum plastic shear resistance, V_u

$$V_u = \frac{M_{pa}}{(g_{2a}/2)} \qquad \text{(k/in)}$$

Total shear resistance of each web angle, V_a

$$V_a = \frac{L_a V_u}{2} \qquad \text{(k)}$$

Although the internal flexural span of the angles is calculated exactly the same in the simplified models for top and seat angle connections and double web angle connections, the value of g_{2a} is used only to calculate the shear resistance at the top of the web angles, V_u. From this maximum shear resistance value V_u, which occurs at the top of the angles, the shear resistance distribution is assumed to diminish linearly to zero at the bottom of the angles. The result is a triangular shear resistance distribution as shown in Figure B.4.

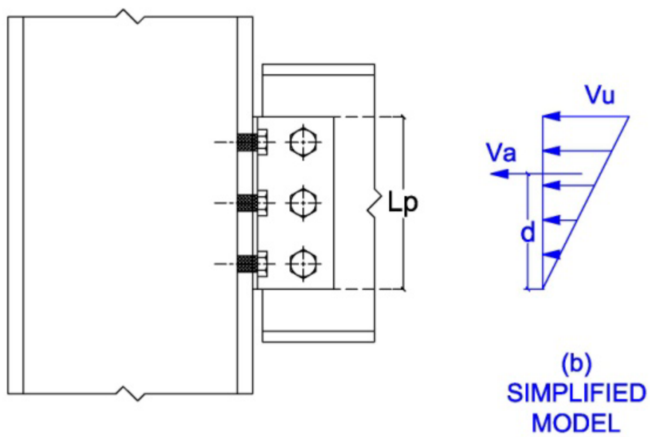

Figure B.4. Assumed shear resistance of double web angles (Simplified model)

Calculate ultimate moment capacity.

The distance between the assumed center of rotation (the bottom of the angles) and the centroid of the shear resistance distribution, d_3, is the moment arm over which V_a acts. The ultimate moment capacity for a single web angle is the product of V_a and d_3; M_u of the entire double angle connection is twice the resistance of a single angle.

$d_3 = \frac{2}{3} L_p$ (in)

$M_u = 2V_a d_3 = \frac{2}{3} V_u {L_a}^2$ (k-in)

Example B.2

Determine relevant connection parameters.

Connection geometry from Abolmaali et al (2003) - Specimen DW-BB-4

$L_a = 14.5$ in

$t_a = 0.25$ in

$k_a = 0.625$ in

$g_{ca} = 2.1$ in

$\sigma_{ya} = 57$ ksi

$w_a = 1.25$ in

Calculate internal flexural span.

$$g_{2a} = g_{ca} - k_a - \frac{w_a}{2} = 2.1 \text{ in} - 0.625 \text{ in} - \frac{1.25 \text{ in}}{2} = 0.85 \text{ in}$$

Determine shear resistance.

$$M_{pa} = \frac{t_a{}^2 \sigma_{ya}}{4} = \frac{(0.25\ \text{in}^2\ )(57\ \text{ksi}\ )}{4} = \ 0.891\ \frac{\text{k-in}}{\text{in}}$$

$$V_u = \frac{M_{pa}}{(g_{2a}/2)} = \frac{\left(0.891\ \frac{\text{k-in}}{\text{in}}\right)}{(0.85\ \text{in}/2)} = 2.10\ \frac{\text{k}}{\text{in}}$$

$$V_a = \frac{L_a V_u}{2} = \frac{(14.5\ \text{in})(2.10\ \text{k/in})}{2} = 15.2\ \text{k}$$

Calculate ultimate moment capacity.

$$M_u \ = \frac{2}{3} V_u L_a{}^2 \ = \frac{2}{3}(2.10\ \text{k/in})(14.5\ \text{in})^2 \ = \ 294\ \text{k-in} \ = \ \boxed{24.5\ \text{k-ft}}$$

Example B.3

Determine relevant connection parameters.

Connection geometry from Abolmaali et al (2003) - Specimen DW-BB-5

L_a = 14.5 in

t_a = 0.375 in

k_a = 0.75 in

g_{ca} = 2.1 in

σ_{ya} = 52 ksi

$w_a = 1.25$ in

Calculate internal flexural span.

$$g_{2a} = g_{ca} - k_a - \frac{w_a}{2} = 2.1 \text{ in} - 0.75 \text{ in} - \frac{1.25 \text{ in}}{2} = 0.725 \text{ in}$$

Determine shear resistance.

$$M_{pa} = \frac{{t_a}^2 \sigma_{ya}}{4} = \frac{(0.375 \text{ in}^2)(52 \text{ ksi})}{4} = 1.83 \ \frac{\text{k-in}}{\text{in}}$$

$$V_u = \frac{M_{pa}}{(g_{2a}/2)} = \frac{\left(1.83 \frac{\text{k-in}}{\text{in}}\right)}{(0.725 \text{ in}/2)} = 5.04 \ \frac{\text{k}}{\text{in}}$$

$$V_a = \frac{L_a V_u}{2} = \frac{(14.5 \text{ in})(5.04 \text{ k/in})}{2} = 36.6 \text{ k}$$

Calculate ultimate moment capacity.

$$d_3 = \frac{2}{3} L_p = \frac{2}{3}(14.5 \text{ in}) = 9.67 \text{ in}$$

$$M_u = \frac{2}{3} V_u {L_a}^2 = \frac{2}{3}(5.04 \text{ k/in})(14.5 \text{ in})^2 = 707 \text{ k-in} = \boxed{59.0 \text{ k-ft}}$$

Appendix C

Appendix C describes two models used for the prediction of ultimate moment capacity for Type 2 connections.

C.1. Chen's Model

Calculate internal flexural span.

$$g_{2t} = g_{ct} - k_t - \frac{w_t}{2} - \frac{t_t}{2} \qquad \text{(in)} \qquad \textit{Top and seat angles}$$

$$g_{2a} = g_{ca} - k_a \qquad \text{(in)} \qquad \textit{Double web angles}$$

Determine shear resistance.

Top and Seat Angles

Maximum plastic shear resistance, V_{ot} (pure shear)

$$V_{ot} = \frac{L_t t_t \sigma_{yt}}{2} \qquad \text{(k)}$$

Plastic shear resistance, V_{pt} (shear and flexure)

$$\left(\frac{V_{pt}}{V_{ot}}\right)^4 + \frac{g_{2t}}{t_t}\left(\frac{V_{pt}}{V_{ot}}\right) - 1 = 0$$

Solve the fourth order equation for V_{pt} (k)

Double Web Angles

Maximum plastic shear resistance, V_{oa} (pure shear)

$$V_{oa} = \frac{L_a t_a \sigma_{ya}}{2} \qquad \text{(k/in)}$$

Minimum plastic shear resistance, V_{pu} (shear and flexure)

$$\left(\frac{V_{pu}}{V_{oa}}\right)^4 + \frac{g_{2a}}{t_a}\left(\frac{V_{pu}}{V_{oa}}\right) - 1 = 0$$

Solve the fourth order equation for V_{pu} (k/in)

Total shear resistance of each web angle, V_a

$$V_a = \frac{L_a(V_{pu}+V_{oa})}{2} \qquad \text{(k)}$$

Calculate ultimate moment capacity.

To calculate M_u for Type 2 connections, Chen's model sums all the contributing components from the separate angles (top, seat, and web). These components are represented by the moment capacities from the bending of the seat angle (M_{os}), the bending of the top angle (M_{pt}), the shear on the top angle ($V_{pt}d_2$), and the shear of the double web angles ($2V_a d_4$).

Plastic moment capacity of seat angle, M_{os}

$$M_{os} = \frac{L_t t_t^2 \sigma_{yt}}{4} \qquad \text{(k-in)}$$

Plastic moment capacity of secondary hinge in top angle, M_{pt}

$$M_{pt} = \frac{V_{pt} g_{2t}}{2} \qquad \text{(k-in)}$$

Ultimate moment of connection, M_u

$$M_u = M_{os} + M_{pt} + V_{pt} d_2 + 2V_a d_4 \qquad \text{(k-in)}$$

where $d_2 = d + \frac{t_t}{2} + k_t$ (in)

$$d_4 = \frac{L_p(2V_{pu} + V_{oa})}{3(V_{pu} + V_{oa})} + \frac{d - L_p}{2} + \frac{t_t}{2} \qquad \text{(in)}$$

The variable d_2 describes the distance from the center of rotation to the line of action of V_{pt}, and d_4 is the distance from the center of rotation to V_a. $V_{pt}d_2$ is the plastic moment capacity of the primary hinge in the top angle. $2V_a d_4$ is the plastic moment capacity of the double web angles.

Example C.1

Determine relevant connection parameters.

Connection geometry from Azizinamini et al (1985) - Specimen 8S4

d = 8.28 in

Top, seat angles: L_t = 6.0 in Web angles: L_a = 5.5 in

$t_t = 0.375$ in | $t_a = 0.25$ in

$k_t = 0.875$ in | $k_a = 0.625$ in

$g_{ct} = 4.5$ in | $g_{ca} = 2.59$ in

$\sigma_{yt} = 40.6$ ksi | $\sigma_{ya} = 40$ ksi

$w_t = 1.25$ in | $w_a = 1.25$ in

Calculate internal flexural spans.

$$g_{2t} = g_{ct} - k_t - \frac{w_t}{2} - \frac{t_t}{2} = 4.5 \text{ in} - 0.875 - \frac{1.25 \text{ in}}{2} - \frac{0.375 \text{ in}}{2} = 2.8125 \text{ in}$$

$$g_y = g_{ca} - k_a = 2.59 \text{ in} - 0.625 \text{ in} = 1.965 \text{ in}$$

Determine shear resistance.

Top and Seat Angles

$$V_{ot} = \frac{L_t t_t \sigma_{yt}}{2} = \frac{(6.0 \text{ in})(0.375 \text{ in})(40.6 \text{ ksi})}{2} = 45.675 \text{ k}$$

$$\left(\frac{V_{pt}}{V_{ot}}\right)^4 + \frac{g_{2t}}{t_t}\left(\frac{V_{pt}}{V_{ot}}\right) - 1 = \left(\frac{V_{pt}}{45.675 \text{ k}}\right)^4 + \frac{2.8125 \text{ in}}{0.375 \text{ in}}\left(\frac{V_{pt}}{45.675 \text{ k}}\right) - 1 = 0$$

Solve fourth order equation → $V_{pt} = 6.1$ k

Double Web Angles

$$V_{oa} = \frac{t_a \sigma_{ya}}{2} = \frac{(0.25 \text{ in})(40 \text{ ksi})}{2} = 5 \text{ k/in}$$

$$\left(\frac{V_{pu}}{V_{oa}}\right)^4 + \frac{g_y}{t_a}\left(\frac{V_{pu}}{V_{oa}}\right) - 1 = \left(\frac{V_{pu}}{5\text{ k/in}}\right)^4 + \frac{1.965\text{ in}}{0.25\text{ in}}\left(\frac{V_{pu}}{27.5\text{ k}}\right) - 1 = 0$$

Solve fourth order equation → V_{pu} = 0.63 k/in

$$V_a = \frac{L_a(V_{pu}+V_{oa})}{2} = \frac{(5.5\text{ in})(0.63\text{ k/in}+5\text{ k/in})}{2} = 15.5\text{ k}$$

Calculate ultimate moment capacity.

$$M_{os} = \frac{L_t t_t{}^2 \sigma_{yt}}{4} = \frac{(6.0\text{ in})(0.375\text{ in})^2(40.6\text{ ksi})}{4} = 8.564\text{ k-in} = 0.71\text{ k-ft}$$

$$M_{pt} = \frac{V_{pt} g_{2t}}{2} = \frac{(6\text{ k})(2.8125\text{ in})}{2} = 8.4375\text{ k-in} = 0.70\text{ k-ft}$$

$$d_2 = d + \frac{t_t}{2} + k_t = (8.28\text{ in}) + \left(\frac{0.375\text{ in}}{2}\right) + (0.875\text{ in}) = 9.3425\text{ in}$$

$$V_{pt} d_2 = (6.1\text{ k})(9.3425\text{ in}) = 57\text{ k-in} = 4.75\text{ k-ft}$$

$$d_4 = \frac{L_p(2V_{pu}+V_{oa})}{3(V_{pu}+V_{oa})} + \frac{d-L_p}{2} + \frac{t_t}{2} = \frac{(5.5\text{ in})(2*0.63\text{ k}+5\text{ k})}{3(0.63\text{ k}+5\text{ k})} + \frac{8.28\text{ in}-5.5\text{ in}}{2} + \frac{0.375\text{ in}}{2} = 3.62\text{ in}$$

$$2V_a d_4 = 2(15.5\text{ k})(3.62\text{ in}) = 112\text{ k-in} = 9.35\text{ k-ft}$$

$$M_u = M_{os} + M_{pt} + V_{pt} d_2 + 2V_a d_4 = 0.71\text{ k-ft} + 0.70\text{ k-ft} + 4.75\text{ k-ft} + 9.35\text{ k-ft} = \boxed{15.5\text{ k-ft}}$$

C.2. Simplified Model

Calculate internal flexural span.

$$g_{2t} = g_{ct} - k_t - \frac{w_t}{2}$$ (in) *Top and seat angles*

$$g_{2a} = g_{ca} - k_a - \frac{w_a}{2}$$ (in) *Double web angles*

Determine shear resistance.

Top and Seat Angles

Maximum plastic moment resistance, M_{pt}

$$M_{pt} = Z_t \sigma_{yt} = \frac{L_t {t_t}^2 \sigma_{yt}}{4}$$ (k-in)

Plastic shear resistance, V_{pt}

$$V_{pt} = \frac{M_{pt}}{(g_{2t}/2)}$$ (k)

Double Web Angles

The simplified model for Type 2 connections is essentially a combination of the simplified models for top and seat angle connections and double web angle connections. However, the centers of rotation for the top and seat angle connection and double web angle connection are not located at the same point; the top and seat angle model assumes a center of rotation within the heel of the seat angle, while the double web angle model assumes a center of rotation at the bottom of the angles.

In this model, the center of rotation is once again assumed to be located at the heel of the seat angle; therefore, the model used for calculating shear resistance in the double web angles needs to be modified slightly to account for this discrepancy. Figure C.1 illustrates the assumptions made for the distribution of shear resistance in the double web angles for the Type 2 connection simplified model. The distribution is assumed to be linear from a maximum value, V_u, at the top of the angles, to zero at the center of rotation. While V_u is calculated exactly the same as in the simplified model for the first two connections, this model also requires computation of the shear resistance at the bottom of the angle, V_1. V_1 can be determined using simple geometry and similar triangles.

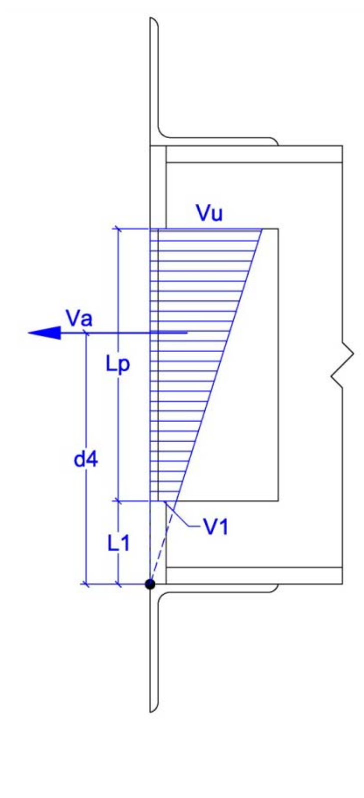

Figure C.1. Shear distribution in web angles for Type 2 connections (simplified model).

The resulting shear resistance distribution is slightly different than the simplified model for double web angle connections, but provides a larger contribution to the ultimate moment capacity.

Maximum plastic moment resistance, M_{pa}

$$M_{pa} = Z_a \sigma_{ya} = \frac{{t_a}^2 \sigma_{ya}}{4} \qquad \text{(k-in/in)}$$

Maximum plastic shear resistance, V_u

$$V_u = \frac{M_{pa}}{(g_{2a}/2)} \qquad \text{(k/in)}$$

Minimum shear on angle, V_1

$$V_1 = \frac{V_u L_1}{L_a + L_1} \qquad \text{(k/in)}$$

where $L_1 = \frac{d - L_a}{2}$ (in)

Total shear resistance of each web angle, V_a

$$V_a = \frac{{L_a}^2 (V_u + V_1)}{2} \qquad \text{(k)}$$

Calculate ultimate moment capacity

Ultimate moment of connection, M_u

$M_u = V_{pt} d_2 + 2V_a d_4$ (k-in)

where $d_4 = \frac{L_a(2V_u+V_1)}{3(V_u+V_1)} + L_1$ (in)

$d_2 = d + g_{ct}$ (in)

The variable d_4 is the distance from the center of rotation to V_a. $V_{pt}d_2$ is the plastic moment capacity of the primary hinge in the top angle. $2V_a d_4$ is the plastic moment capacity of the double web angles.

Example C.2

Determine relevant connection parameters.

Connection geometry from Azizinamini et al (1985) – Specimen 8S4

d = 8.28 in

Top, seat angles:	L_t = 6.0 in	Web angles:	L_a = 5.5 in
	t_t = 0.375 in		t_a = 0.25 in
	k_t = 0.875 in		k_a = 0.625 in
	g_{ct} = 4.5 in		g_{ca} = 2.59 in
	σ_{yt} = 40.6 ksi		σ_{ya} = 40 ksi

$w_t = 1.25$ in $\qquad\qquad$ $w_a = 1.25$ in

Calculate internal flexural spans.

$$g_{2t} = g_{ct} - k_t - \frac{w_t}{2} = 4.5 \text{ in} - 0.875 \text{ in} - \frac{1.25 \text{ in}}{2} = 3.00 \text{ in}$$

$$g_{2a} = g_{ca} - k_a - \frac{w_a}{2} = 2.59 \text{ in} - 0.625 \text{ in} - \frac{1.25 \text{ in}}{2} = 1.34 \text{ in}$$

Determine shear resistance.

Top and Seat Angles

$$M_{pt} = \frac{L_t {t_t}^2 \sigma_{yt}}{4} = \frac{(6.0 \text{ in})(0.375 \text{ in})^2(40.6 \text{ ksi})}{4} = 8.56 \text{ k-in}$$

$$V_{pt} = \frac{M_{pt}}{(g_{2t}/2)} = \frac{8.56 \text{ k-in}}{(3.00 \text{ in}/2)} = 5.7 \text{ k}$$

Double Web Angles

$$M_{pa} = \frac{{t_a}^2 \sigma_y}{4} = \frac{(0.25 \text{ in})^2(40 \text{ ksi})}{4} = 0.625 \ \frac{\text{k-in}}{\text{in}}$$

$$V_u = \frac{M_{pa}}{(g_{2a}/2)} = \frac{0.625 \ \frac{k-in}{\text{in}}}{(1.34 \text{ in}/2)} = 0.932 \ \frac{\text{k}}{\text{in}}$$

$$L_1 = \frac{d - L_a}{2} = \frac{8.28 \text{ in} - 5.5 \text{ in}}{2} = 1.39 \text{ in}$$

$$V_1 = \frac{V_u L_1}{L_a + L_1} = \frac{\left(0.932 \frac{\text{k}}{\text{in}}\right)(1.39 \text{ in})}{(5.5 \text{ in}) + (1.39 \text{ in})} = 0.188 \text{ k}$$

$$V_a = \frac{{L_a}^2(V_u+V_1)}{2} = \frac{(5.5\text{ in})^2\left(0.932\,\frac{\text{k}}{\text{in}}+0.188\,\frac{\text{k}}{\text{in}}\right)}{2} = 16.9\text{ k}$$

Calculate ultimate moment capacity.

$$d_2 = 8.28\text{ in} + 4.5\text{ in} = 12.8\text{ in}$$

$$V_{pt}d_2 = (5.7\text{ k})(12.8\text{ in}) = 73\text{ k-in} = 6.0\text{ k-ft}$$

$$d_4 = \frac{L_a(2V_u+V_1)}{3(V_u+V_1)} + L_1 = \frac{(5.5\text{ in})(2*5.13\text{ k}+1.03\text{ k})}{3(5.13\text{ k}+1.03\text{ k})} + 1.39\text{ in} = 4.75\text{ in}$$

$$2V_a d_4 = 2(16.9\text{ k})(4.75\text{ in}) = 160.6\text{ k-in} = 13.4\text{ k-ft}$$

$$M_u = V_{pt}d + 2V_a d_4 = 6.0\text{ k-ft} + 13.4\text{ k-ft} = \boxed{19.4\text{ k-ft}}$$

Appendix D

Author	Year	Publication	Comments
Top- and Seat-Angles with Double Web Angles			
Reviewed			
Disque	1976	*Type 2 Construction* Publication	Explanation of Type II construction
Azizinamini et al	1985	National Science Foundation report	Comprehensive report on testing program
Azizinamini et al	1987	Journal of Constructional Steel Research	Same testing program as Azizinamini et al (1985)
Azizinamini et al	1989	Journal of Structural Engineering	Same testing program as Azizinamini et al (1985)
Chen	2000	Practical Analysis of Semi-Rigid Connections	Introduces methods of analysis for many semi-rigid connection types, including ultimate moment predictions
To Be Reviewed			
Rathbun	1936	Trans. ASCE	
Hechtman et al	1947	AISC research report	
Bose	1981	Journal of the Institution of Engineers (India)	
Maxwell et al	1981	Joints in Structural Steelwork	
Radziminski et al	1986	Proceedings of the 3rd U.S. National Conference on Earthquake Engineering	Same testing program as Azizinamini et al (1985)
Roeder et al	1996	Journal of Structural Engineering	No original testing program
Liew et al	1997		
Oosterhof et al	2012		
Not to Review			
Kasai et al	2000	Behaviour of Steel Structures in Seismic Areas	Fillet weld at toe of top angle; long-slotted holes
Double Angles			
Reviewed			
Abolmaali et al	2003	Journal of Constructional Steel Research	Five specimens excluded (welded-bolted)
To Be Reviewed			
Rathbun	1936	Trans. ASCE	
Hechtman et al	1947	AISC research report	
Bell	1957	Thesis, University of Illinois Urbana-Champaign	
Sommer	1969	Thesis, University of Toronto	
Bose	1981	Journal of the Institution of Engineers (India)	
Maxwell et al	1981	Joints in Structural Steelwork	
Radziminski et al	1986	Proceedings of the 3rd U.S. National Conference on Earthquake Engineering	Same testing program as Azizinamini et al (1985)
Yang et al	2012		
Not to Review			
Munse et al	1959	Journal of the Structural Division	Double bolt rows on beam flange
Lewitt et al	1966	University of Illinois Urbana-Champaign	Double bolt rows on beam flange
Leon et al	1987	AISC Engineering Journal	Composite
Astaneh et al	1989	AISC Engineering Journal	Welded-bolted connections
Jaspart et al	1990	International Association for Bridge and Structural Engineers	Composite
Ammerman et al	2003		Composite

Top and Seat Angle			
Reviewed			
Kukreti et al	1999	Journal of Structural Engineering	Six specimens excluded (bolt failure)
Garlock	2003	Journal of Structural Engineering	Pull tests on angles
Eurocode 3	2005	Eurocode 3	European Design Standard
To Be Reviewed			
Stelmack et al	1986	Journal of Structural Engineering	
Design/Analysis Methodology & Models			
Reviewed			
Chen	1989	Journal of Structural Engineering	Purdue Steel Connection Data Base
Kishi et al	1990	Journal of Structural Engineering	Analysis of semi-rigid connections
To Be Reviewed			
Johnston	1940	Engineering News-Record	Design economy
Lionberger	1969	Journal of Engineering Mechanics Division	Frames
Grundy et al	1980	ASCE Engineering Journal	
Ackroyd et al	1982	ASCE Journal of the Structural Division	Type II frames
Morris et al	1986	Canadian Journal of Civil Engineering	Frames
Cook	1987	Journal of Structural Engineering	Type II frames
Gerstle et al	1987	Engineering Structures	Frames
Kishi et al	1987	Proceedings: Structures Congress '87	Purdue Steel Connection Data Base
Lui et al	1987	Journal of Constructional Steel Research	Frames
Gerstle	1988	Journal of Constructional Steel Research	Frames
Shing et al	1989	Proceedings: Structures Congress '89	Frames
Gerstle et al	1990	AISC Engineering Journal	Frames
Roeder et al	1996	Journal of Structural Engineering	Type II
Kishi et al	2001	Structural Engineering and Mechanics	Finite element analysis
Not to Review			
Attiogbe et al	1991	Journal of Structural Engineering	Data regression
Chen et al	2001		Finite element analysis; T&S/DW
Kishi et al	2001	Structural Engineering and Mechanics	Finite element analysis; T&S/DW
Lee et al	2001	Engineering Structures	Analytical model; T&S/DW
Danesh et al	2006		Finite element analysis; initial stiffness; T&S/DW
Pirmoz et al	2009	Journal of Constructional Steel Research	Finite element analysis; T&S/DW
Diaz et al	2011	Journal of Constructional Steel Research	Review of analytical models

KEY

T&S: Top and seat angle connections

DW: Double web angle connections

T&S/DW: Top and seat with double web angle connections